Article

ESR1 and p53 interactome alteration defines mechanisms of tamoxifen response in luminal breast cancer

Window-of-Opportunity Trial in ERα+ Breast Cancer

No Tamoxifen intervention — Tamoxifen intervention

ERα / ERE

ERα-p53 interaction — ERα / WTp53 / p53 binding site — Inactive p53 — Oncogenic program

No ERα-p53 interaction — ERα / WTp53 / p53 binding site — Active p53 leading to transcriptional reprogramming — Tumor suppression program

Chetan C. Oturkar, Spencer R. Rosario, Alan D. Hutson, ..., Andrew K.L. Goey, Swati Kulkarni, Gokul M. Das

skulkarn@nm.org (S.K.)
gokul.das@roswellpark.org (G.M.D.)

Highlights

A window-of-opportunity clinical trial in newly diagnosed ERα (ESR1) + breast cancer patients

Inhibition of ESR1-p53 interaction in tumors by tamoxifen has clinical implications

Reactivation of wild-type p53 by tamoxifen leads to tumor-suppressive gene expression

p53 reactivation is associated with mevalonate pathway repression signature

Article

ESR1 and p53 interactome alteration defines mechanisms of tamoxifen response in luminal breast cancer

Chetan C. Oturkar,[1,8] Spencer R. Rosario,[2,8] Alan D. Hutson,[2] Adrianne Groman,[2] Stephen B. Edge,[3] Carl D. Morrison,[4] Wendy M. Swetzig,[1] Jianmin Wang,[2] Jun Hyoung Park,[5] Benny Abraham Kaipparettu,[5] Prashant K. Singh,[6] Shicha Kumar,[3] Helen H. Cappuccino,[3] Manish Ranjan,[7] Araba Adjei,[1] Mohammad Ghasemi,[1] Andrew K.L. Goey,[1] Swati Kulkarni,[7,*] and Gokul M. Das[1,9,*]

SUMMARY

The canonical mechanism behind tamoxifen's therapeutic effect on estrogen receptor α/ESR1+ breast cancers is inhibition of ESR1-dependent estrogen signaling. Although ESR1+ tumors expressing wild-type p53 were reported to be more responsive to tamoxifen (Tam) therapy, p53 has not been factored into choice of this therapy and the mechanism underlying the role of p53 in Tam response remains unclear. In a window-of-opportunity trial on patients with newly diagnosed stage I–III ESR1+/HER2/wild-type p53 breast cancer who were randomized to arms with or without Tam prior to surgery, we reveal that the ESR1-p53 interaction in tumors was inhibited by Tam. This resulted in functional reactivation of p53 leading to transcriptional reprogramming that favors tumor-suppressive signaling, as well as downregulation of oncogenic pathways. These findings illustrating the convergence of ESR1 and p53 signaling during Tam therapy enrich mechanistic understanding of the impact of p53 on the response to Tam therapy.

INTRODUCTION

The incidence of premenopausal breast cancer is increasing worldwide.[1] Approximately 650,000 premenopausal women are diagnosed each year and 130,000 die from their disease. In the United States, it is the most commonly diagnosed cancer and the leading cause of death in women under 50. The majority of these premenopausal breast cancers are estrogen receptor α-positive (ESR1+). Treatment of these cancers has historically centered on medications such as tamoxifen (Tam) that inhibit activation of ESR1.[2,3] It is widely accepted that Tam, a selective estrogen receptor modulator (SERM), exerts its therapeutic effect by competitively binding to ESR1 to prevent the transcription of genes involved in the proliferation of breast cancer epithelium. Numerous clinical studies have shown that Tam is highly effective in the treatment of breast cancer. The Early Breast Cancer Trialists' Collaborative Group meta-analysis of 55 clinical trials with 30,000 women reported that five years of Tam reduced the risk of breast cancer recurrence by 47% and the risk of death from breast cancer by 26%.[4] Extending Tam treatment for ten years further decreased the risk of recurrence and risk of death from breast cancer.[5] Moreover, Tam reduces the risk of developing breast cancer by 50% in women at high risk.[6] Since the discovery of Tam as an effective SERM for treatment for ESR1+ breast cancer, several other medications have been developed to target ESR1+ breast cancer, including aromatase inhibitors (AIs), selective estrogen receptor disrupters, and CDK4/6 inhibitors. As absolute benefit from therapy is related to risk, the added benefit of AIs over Tam is small in low-risk patients, and even in higher-risk women, intolerance of an AI is a good reason to consider Tam as a therapeutic option.[7] According to the 2023 NCCN's national clinical practice guidelines on breast cancer, Tam remains the first-line adjuvant treatment for premenopausal women with early-stage, low-risk ESR1+/human epidermal growth factor receptor (HER)– breast cancer[8]

The tumor suppressor protein p53 promotes cell-cycle arrest, senescence, and apoptosis in response to various stress signals and genomic damages. Inactivation of p53 in tumors occurs because of mutations that disable binding to the appropriate target gene promoters or altered interaction with other protein partners.[9,10] Unlike ESR1-negative tumors, most ESR1+ breast tumors express wild-type

[1]Department of Pharmacology and Therapeutics, Roswell Park Comprehensive Cancer Center, Buffalo, NY, USA
[2]Department of Biostatistics and Bioinformatics, Roswell Park Comprehensive Cancer Center, Buffalo, NY, USA
[3]Department of Breast Surgery, Roswell Park Comprehensive Cancer Center, Buffalo, NY, USA
[4]Department of Pathology, Roswell Park Comprehensive Cancer Center, Buffalo, NY, USA
[5]Department of Molecular and Human Genetics, Baylor College of Medicine, Houston, TX, USA
[6]Department of Cancer Genetics and Genomics, Roswell Park Comprehensive Cancer Center, Buffalo, NY, USA
[7]Division of Breast Surgery, Northwestern University Feinberg School of Medicine, Robert H. Lurie Comprehensive Cancer Center, Chicago, IL, USA
[8]These authors contributed equally
[9]Lead contact
*Correspondence: skulkarn@nm.org (S.K.), gokul.das@roswellpark.org (G.M.D.)
https://doi.org/10.1016/j.isci.2024.109995
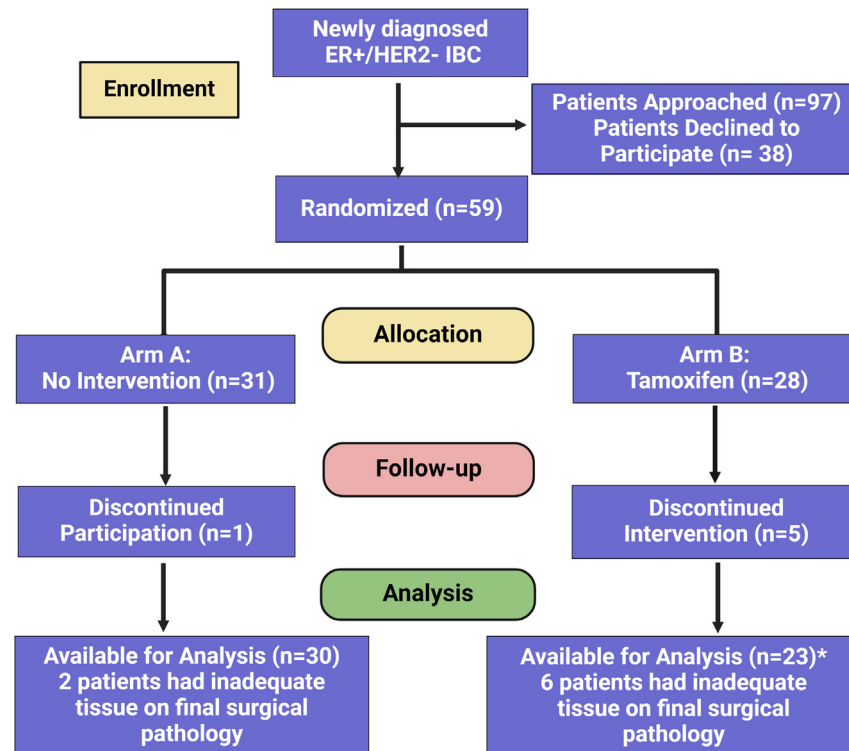
Figure 1. Consort diagram of the clinical trial
See also Tables S1–S3.

p53. However, in the majority of ESR1+ tumors, p53 is functionally inactive as a tumor suppressor. Our pre-clinical studies showed that ESR1 binds to wild-type p53 *in vitro*[11] and *in vivo* in breast cancer xenograft models[12] and represses p53-target genes by recruiting co-repressors, leading to the downregulation of apoptosis.[13] Previous clinical studies in patients with ESR1+ tumors have shown that those with wild-type p53 (determined by DNA sequencing) tumors were more responsive to adjuvant Tam therapy leading to better overall survival and progression-free survival[14,15] compared to patients with tumors expressing mutant p53. In 846 patients treated with Tam for 5 years in the International Breast Cancer Study Group Trials VIII and IX, wild-type p53 (as determined by immunohistochemistry) was associated with increased disease-free survival and overall survival in patients with ESR1+ breast cancer.[16] In addition, in ESR1+ breast cancer, functional p53 deficiency, as assessed by gene expression readout, was shown to be predictive of resistance to Tam in terms of shorter disease-specific survival.[17] However, the mechanism underlying the increased responsiveness of ESR1+ tumors expressing wild-type p53 to Tam remains elusive. This lack of information precludes the use of p53 expression to identify patients who are most likely to respond to Tam, the most prescribed therapy for premenopausal ESR1+ breast cancer. Here, we provide evidence for a mechanism that is centered on the Tam-mediated reactivation of wild-type p53.

We hypothesized that functional suppression of wild-type p53 by ESR1 is a major mechanism that drives ESR1+/breast cancer in patients. Inhibition of the ESR1-p53 interaction and reactivation of p53 would cause reprogramming of gene expression, leading to the activation of tumor suppressor pathways in patients. We tested this hypothesis in a window-of-opportunity study of women with newly diagnosed ESR1+/ HER− breast cancer. This study had two overarching goals. First, to investigate the status of the ESR1-p53 interaction in ESR1+/wild-type p53 human breast tumors and examine how Tam therapy impacts this interaction. Second, to determine the effect of p53 reactivation by Tam on reprogramming of gene expression in these tumors for the primary purpose of identifying alternative mechanisms that can be targeted for future therapeutic interventions and to determine whether p53 expression can be used for patient stratification and as a predictive marker for Tam therapy.

Women with ESR1+ breast cancer were randomized to receive 20 mg of Tam PO daily for 28 days or no intervention between diagnosis and surgery (Figure 1). Fresh normal and tumor tissues and blood were obtained from patients and analyzed to assess the full biological profile and to create a comprehensive molecular model for patients in these groups. Tumor samples were analyzed to assess Tam metabolite levels (mass spectrometry-based bioanalytics), ESR1-p53 interaction (proximity ligation assay/PLA), transcriptomic changes (RNA sequencing), and protein expression levels (reverse phase protein array/RPPA) (Figure 2). The results of our comprehensive analysis of the effects of Tam treatment on breast cancer patients with ESR1+/wild-type p53 tumors revealed a specific transcriptional and proteomic signature associated with Tam, reflecting changes in tumor suppressor and oncogenic pathways.
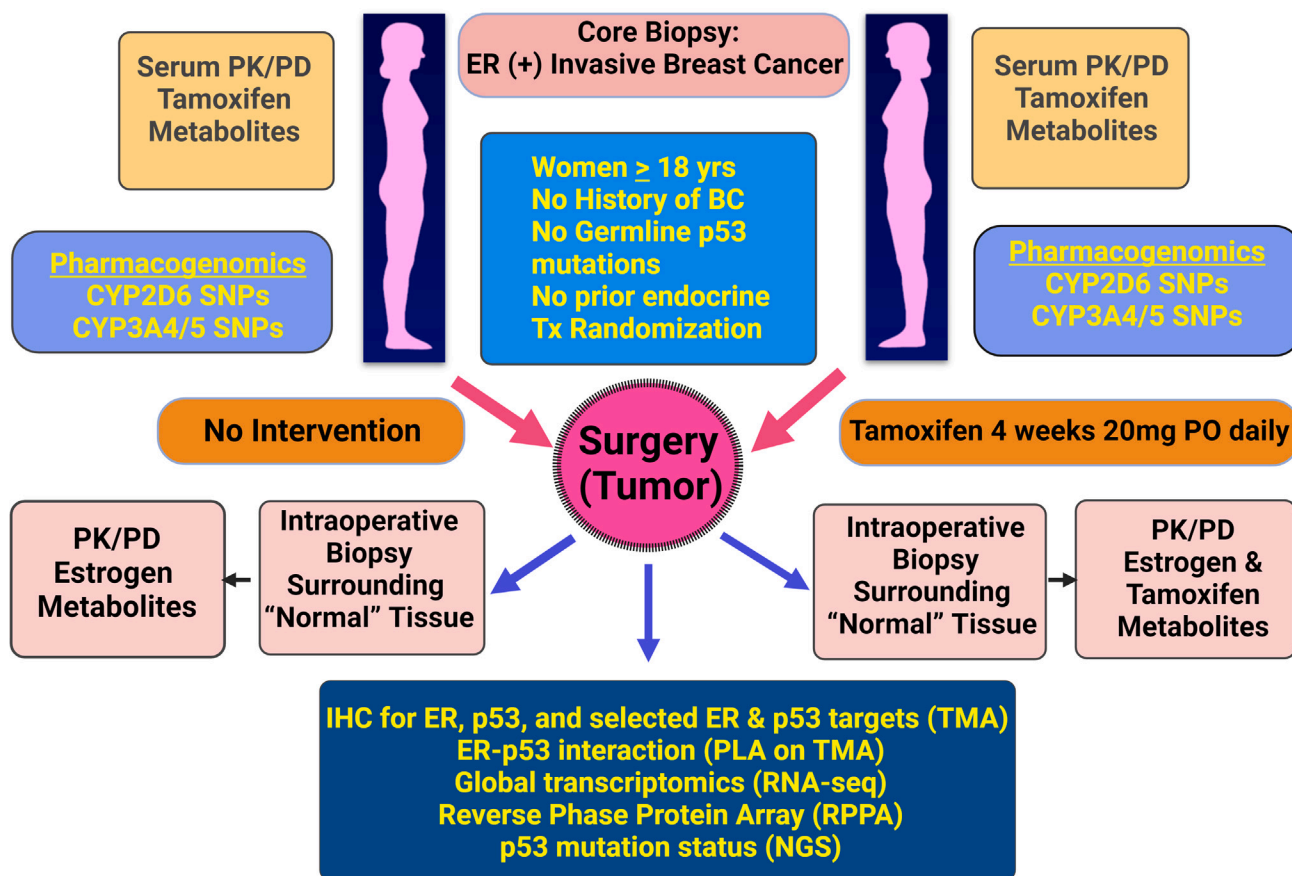
Figure 2. Schema representing study design, eligibility, and endpoints of the clinical trial

RESULTS

Patient demographics

After institutional review board approval at the Roswell Park Comprehensive Cancer Center and the University of Chicago, 59 patients were enrolled in this randomized window-of-opportunity study (NCT01027416) at both institutions between 2010 and 2015. The representativeness of study participants is described in Table S1. Fifty-three patients completed the trial (Figure 1; Table S2). The two arms of the trial were evenly matched by age, race, menopausal status, race, tumor stage, Ki-67 H-score, and Oncotype score (Table S3). Twenty-three (55%) patients had a Ki-67 index below 14. The Oncotype score was evenly split between low and intermediate scores in the 22 (42%) patients who underwent testing. The pathological characteristics presented were obtained from the resected tumor sample. The results described here are based on evaluable tissues for each assay obtained from patients with tumors expressing wild-type p53 (Table S4).

Intervention and sample collection

Women with stage I–III newly diagnosed luminal breast cancer (ESR1+/HER−) diagnosed by core needle biopsy were randomized to Arm A: standard of care without intervention or Arm B: Tam 20 mg PO daily for 28 days immediately preceding primary surgery (Figures 1 and 2). No significant adverse events were observed during the intervention. Fresh frozen tumor tissues and surrounding normal tissues were obtained at the time of surgery. Patients had blood for pharmacokinetic analysis drawn at baseline, mid-treatment, and at the conclusion of therapy to ensure that steady-state levels of Tam and its active metabolites were achieved.

Tam metabolites in tumor tissue and plasma

Consistent with earlier reports,[18] liquid chromatography/tandem mass spectrometry analysis demonstrated substantial concentrations of Tam and its associated metabolites N-desmethyltam (ND-Tam), endoxifen, 4-endoxifen-SO4, and 4-hydroxytam (4-OH-Tam) in tumor tissue and plasma (Figure 3), indicating that adequate levels were present within the tumor to exert its effect upon the transcriptome and proteome. Conversely, we found lower levels of Tam N-oxide in the tumor, as would be expected, given its role as a Tam reservoir.[19] Pharmacokinetic analysis indicated that all patients who received Tam reached therapeutic steady-state plasma concentrations of Tam and its three major
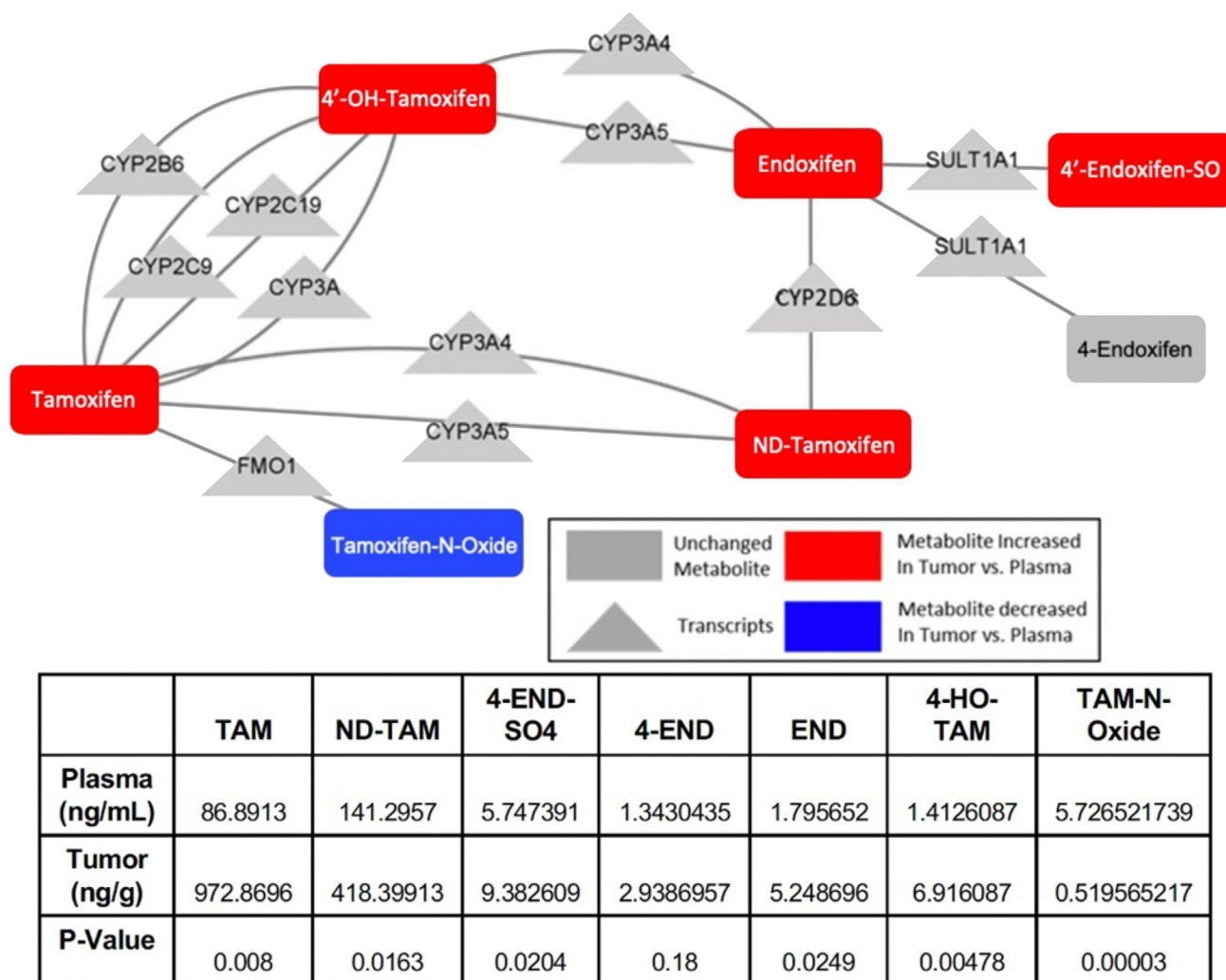
Figure 3. Tamoxifen metabolites in the tumor tissue and plasma

Mass spectrometry-based measurement of key metabolites from the tamoxifen metabolic pathway was measured in patient plasma and tumor samples. Mean abundance in plasma and tumor samples is reported in the table (bottom). *p* value obtained from Student's t test comparing mean plasma and tumor abundance. Network-relating metabolites were constructed (metabolites, rectangles) highlighting metabolites increased in the tumor, as compared to plasma (red), metabolites decreased in the tumor, as compared to the plasma (blue), and metabolites that were not significantly altered between the two sample types (gray). See also Table S4.

metabolites, ND-Tam, 4-OH-Tam, and endoxifen (Figure S4). Covariate analysis of demographic information (i.e., age, sex, height, and body weight), smoking, age after menopause, and CYP2D6 metabolizer status based on *CYP2D6* genotype was performed to identify potential covariates that might contribute to pharmacokinetic variability between subjects. Only body weight met the criteria for inclusion in the final model. Simulated concentration-time profiles showed that the average steady-state plasma concentrations of Tam, 4-OH-Tam, endoxifen, and ND-Tam after repeated dosing of 20 mg Tam/day were similar to values reported in literature[18,20] (Figures S3 and S4). Also, the time to reach steady-state levels of Tam was ~4 weeks, consistent with published data. Based on the estimates of the volume of distribution of Tam and conversion rate constants of Tam to 4-OH-Tam, ND-Tam, Tam-NOX, and 4'-OH-Tam, the mean oral clearance of Tam was 9.35 L/h which is very close to previously reported values 9.64 L/h[21] and 7.2 L/h.[22]

Tam disrupts ESR1-p53 interaction in breast cancer patient tumors

Based on our previous findings in ESR1+ breast cancer cell lines,[11,13] we hypothesized that in patient tumors, functional suppression of p53 by ESR1 is a major mechanism that drives ESR1+ breast cancer growth. Furthermore, we hypothesized that Tam disrupts the ESR1-p53 interaction, leading to the reactivation of p53. *In situ* PLA revealed that the interaction between p53 and ESR1 was disrupted significantly in tumors
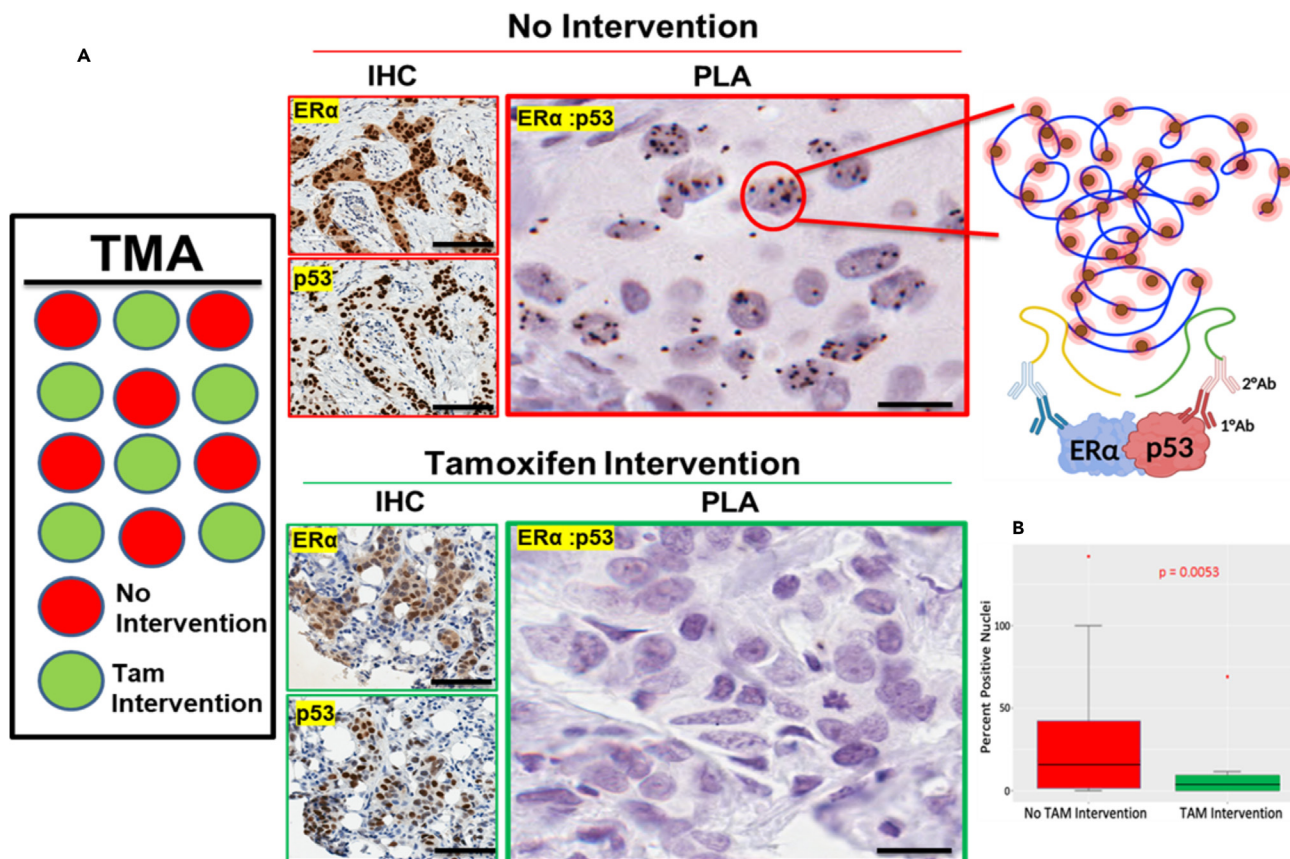
Figure 4. Tamoxifen disrupts ESR1-p53 interaction in breast cancer patient tumors

ESR1-p53 interaction in tamoxifen-treated versus untreated tumor tissue was assayed by bright-field PLA with primary antibodies against ERα (HC20) and p53 (DO1) (Santa Cruz Biotechnology) on breast cancer patient TMA. (A) Representative images of tumor tissue IHC for ERα & p53 and their corresponding PLA interactions are shown.

(B) Quantification of PLA scores for ERα-p53 interaction in tamoxifen-treated vs. untreated tumor is shown on the right panels. Scale bar – PLA, 20 μm and IHC, 100 μm. Data are represented as mean ± SEM. Statistical significance was determined by a Student's t test. *p* = 0.0053. See also Table S4.

from patients treated with Tam as compared with those from treatment-naive patients (Figures 4A and 4B). These data are consistent with the presence of Tam and its metabolites in tumor tissue and plasma (Figure 3) and its steady-state pharmacokinetic profile (Figure S4).

A distinct transcriptomics profile in tumors from Tam-treated versus untreated (standard of care) patients

To determine how Tam affects downstream transcriptional reprograming in the context of p53, we sequenced the RNA of tumor samples from ESR1+/wild-type p53 patients from both arms of the study, which demonstrated a reasonable amount of separation by principal component analysis (untreated [purple] and Tam-treated [green], Figure 5A). Raw feature counts were normalized and differential expression analysis was conducted using "DESeq2" and plotted as volcano plots (Figure 5A) and as a heatmap (Figure 5C). Differentially expressed gene (DEG) analysis of the transcriptional profiles comparing the two treatment arms revealed 307 differentially expressed genes, as defined by a fold change of >1.5, and a *p* value of <0.05 (Figure 5B). These genes provided a reasonable amount of separation by Euclidean distances between the untreated (purple) and Tam-treated (green) samples, as visualized in a heatmap (Figure 5C). One of the most downregulated genes revealed in the volcanic plots (Figure 5B) is a metabolic modulator, 7-dehydrocholesterol reductase (*DHCR7*), which encodes a key enzyme in the mevalonate biosynthetic pathway that synthesizes lipoproteins and cholesterol precursors, and is a known target for repression by wild-type p53.[23] A key upregulated gene was *GJA1*/Connexin 43 (Cx43), a breast tumor suppressor and a predictor of patient survival and distant metastasis-free survival.[24] In addition to being an important component of gap junctions regulating intercellular communication, Cx43 interacts with a variety of proteins.

Global gene set enrichment analysis (GSEA) revealed that the DEGs were functionally enriched for characteristically luminal genes and mammary stem cells (Figures 5D, top and 5E) in the Tam-treatment group. Furthermore, we observed enrichment of signatures that were repressed in ductal carcinoma and matured mammary luminal cells associated with Tam treatment (Figure S1). Conversely, genes associated with high-grade breast cancer and cancer proliferation (Figures 5D, bottom and 5E) as well as genes associated with estradiol response and
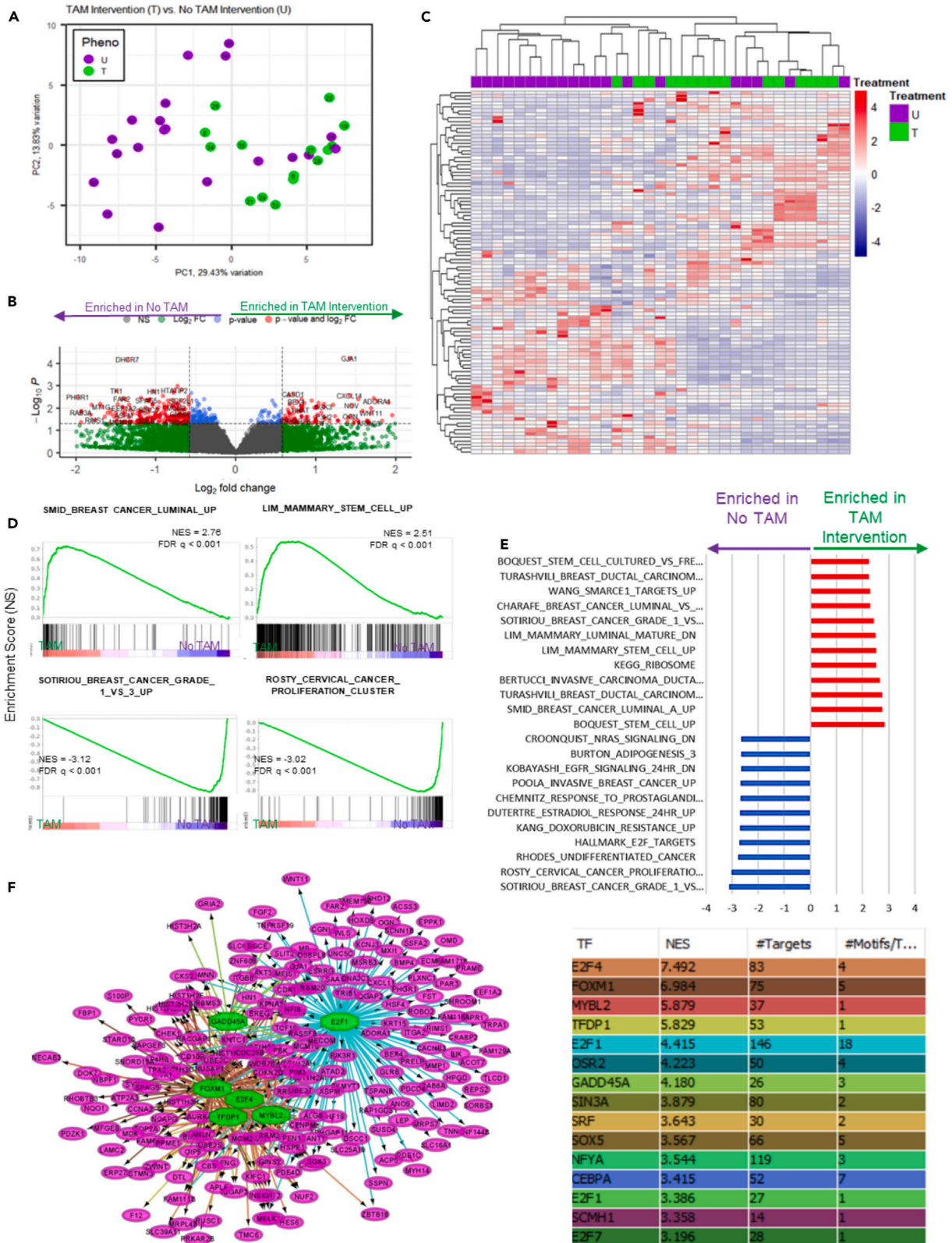
Figure 5. Distinct transcriptomics profile in tumors from tamoxifen-treated versus untreated (standard of care) patients

(A) Principal component analysis of the top 307 differentially expressed genes divided patients into no Tam intervention (U, purple) and Tam-treated groups (T, green) with a good amount of confidence based on a measure of variation using eigen vectors.

(B) The differentially expressed genes (p < 0.05, |logFC|>1.5, red) are displayed in a volcano plot, where upregulated genes in T versus U are to the right, and downregulated genes are to the left.

(C) Heatmap displaying the up- (red) and down- (blue) regulated genes in each cluster. The genes show separation of Tam intervention (T, green) as compared to non-Tam intervention (U, purple) via Euclidean distances.

(D) Representative GSEA plots demonstrating genes enriching for several important and relevant gene sets, such as luminal A and stem cell markers (upper panel) in the treated samples, and high tumor grade and proliferation in the untreated samples (lower panel).

(E) A summary of the normalized enrichment scores (NES) of the top 12 positively (enriched in the treated group, red) and negatively (enriched in the untreated, blue) regulated pathways are plotted and include several pathways involved in epigenetic regulation, cell cycle, and tumor suppressor gene function.

(F) Differentially expressed genes (purple) enriched for master regulators (green) using iRegulon, which were then used to construct a network based on top enrichment scores (left panel), and the number of targets present for each of the master regulators (right panel). See also Figures S1 and S2, and Table S4.

breast cancer relapse (Figure S1) were enriched in the untreated samples. A summary of the normalized enrichment scores (Figure 5E) of the top 12 gene sets enriched in the Tam-treated group (red) included those representing matured luminal cells, stem cells, and low-grade tumors as opposed to high-grade ones. Eleven gene sets enriched in the untreated group (blue) revealed consistent enrichment in metabolic (adipogenesis, prostaglandins, and cholesterol) and proliferative gene sets.

Subsequently, all 307 DEGs, regardless of direction (Figure 5F) and the increased and decreased DEGs separately (Figure S2), were enriched for transcriptional master regulators (MRs) and co-regulated genes using iRegulon.[25] Using these data, we constructed a network based on top enrichment scores (Figure 5F, left panel) and the number of targets present for each of the MRs (Figure 5F, right panel), allowing us to infer the MRs that are associated with the transcriptional alteration occurring as a result of Tam treatment. Network construction revealed several prominent MRs associated with the cell cycle and proliferation such as *E2F1* and *E2F4*, which is consistent with reports on their prognostic significance in breast cancer.[26,27] Not surprisingly, this analysis further revealed known transcriptional targets of activation by ESR1 and repression by wild-type p53. For example, FOXM1, a known inducer of endocrine resistance and invasiveness in ESR1+ breast cancer[28] and a target for p53-mediated transcriptional repression,[29,30] was downregulated in response to Tam treatment. When isolating the MRs of only the downregulated genes, we enriched *MYBL2* (B-myb) (Figure S2), a biomarker for disease severity in breast cancer that correlates with metastasis, early relapse, and shorter overall survival.[31] Furthermore, in isolating the MRs of the upregulated genes (Figure S2), there was enrichment of metabolism-associated *CTBP2* and *JAZF1*, both known to downregulate lipogenic gene expression.[32,33] Overall, the patterns of transcriptomic and MR expression reflect the activation of p53-regulated anti-proliferation, metabolic, and tumor suppression-associated pathways.

Integration of DEGs identified by transcriptomic and proteomic approaches reveals regulatory crosstalk between ESRT1 and p53

To better examine the downstream impacts of Tam treatment on the proteome, we used immunohistochemistry (Figure 6A) and RPPA (Figure 6B) on patient tumor samples. While the levels of nuclear ESR1 and p53 did not change significantly, the prototypic p53-target gene products p21 and MDM2 were significantly upregulated in response to Tam (Figure 6A), consistent with the idea that Tam disrupts the ESR1-p53 interaction, leading to the reactivation of p53 (Figure 4). The RPPA analysis of tumor tissue lysates revealed that 84 out of the 210 proteins probed were significantly dysregulated between the two arms (purple versus green) by both a p value of <0.05 and a fold change of >1.5 (Figure 6B). While the 210 proteins represented a limited set of proteins, functional enrichment of the 84 dysregulated proteins (Figure 6C) revealed key signaling pathways, such as AKT signaling, to be altered. This coincides with alterations in metabolic pathways, given the role that AKT signaling plays in both glucose and lipid metabolism.[34]

Given that there are known post-translational modifications that could result in transcript and protein anti-correlation, we then sought to determine how well the expression of the 84 differentially expressed proteins and their corresponding transcripts correlated with one another (Figure 6D). We identified a small subset of genes that were positively correlated with their protein expression (Figure 6E) and performed a pathway enrichment analysis of this subset. Despite the limited proteomic dataset, we found the largest proportion of genes to be involved in apoptosis, p53 signaling, altered metabolism, and hormonal pathways in breast cancer (Figure 6F), consistent with many of the observed transcriptomic changes.

To better understand the interactome of ESR1 and p53, we created a subnetwork exploring the protein-protein relationship between our smaller subset of differentially expressed proteins, p53 and ESR1, using STRING-db.[35] This subnetwork revealed subsets of proteins associated with p53 (left panel) and ESR1 (right panel) and those co-regulated by both p53 and ESR1 (center panel) (Figure 6G). Furthermore, we integrated the transcriptional information (rim of each oval; higher color intensity of the rim corresponds to higher gene expression and vice versa) of each of the DEGs/proteins, within this subnetwork, revealing a divergence of transcriptomic expression, with roughly half of the genes being transcriptionally increased and half decreased upon Tam treatment. Importantly, we found that when p53 was reactivated in response to Tam therapy, it led to the upregulation of a large array of tumor suppressors and anti-proliferation proteins, with the highest being ID4, PERP, TRIM29, and PDCD41 (Figure 6G). On the other hand, Tam treatment downregulates UBE2C, which is a target for transcriptional repression by p53[36] and facilitates anaphase onset by ubiquitin-mediated degradation of mitotic substrates, leading to chromosome instability in tumors.
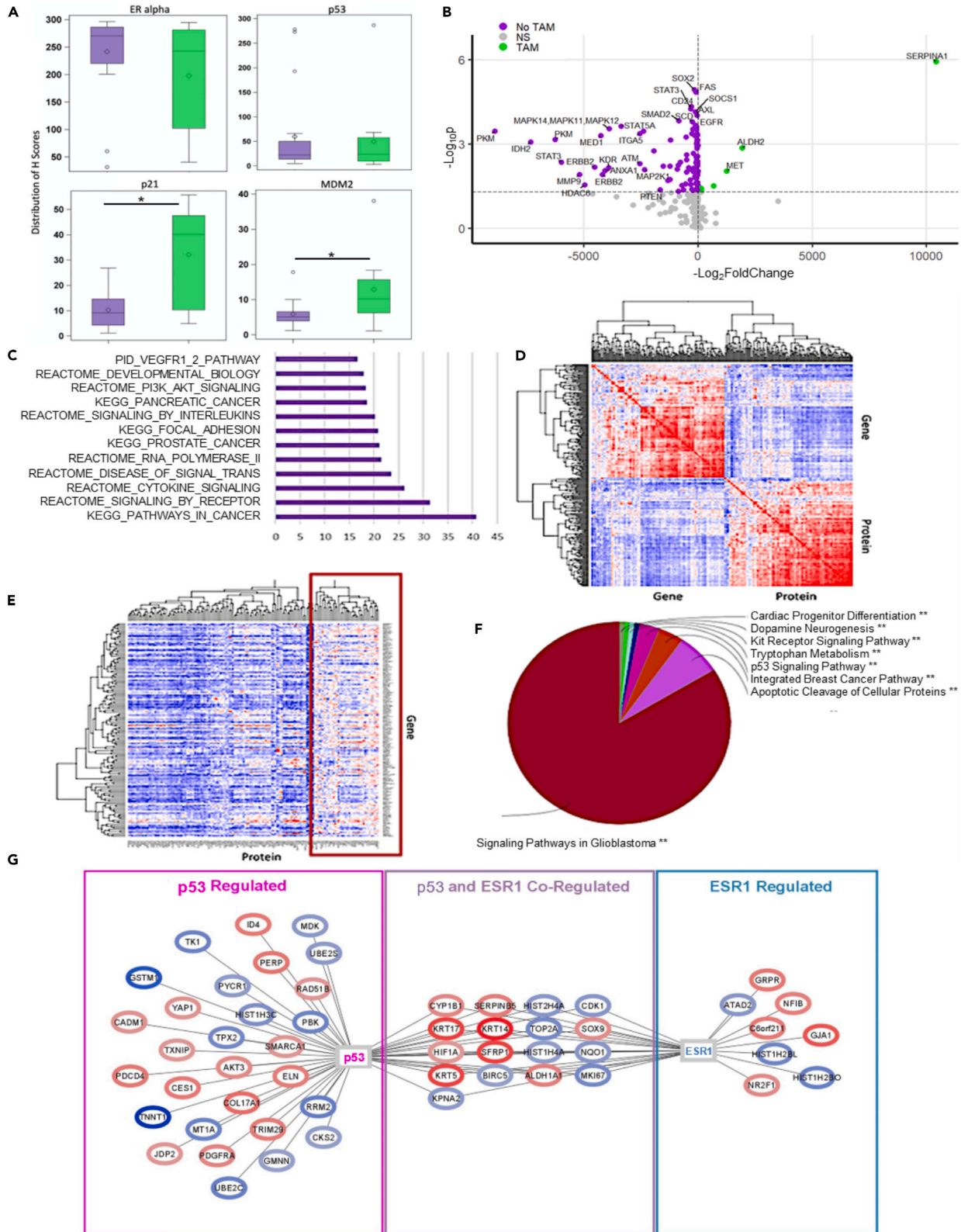
Figure 6. Integration of transcriptomics and proteomics reveals regulatory crosstalk between ESR1 and p53

(A) To assess differential protein expression in response to tamoxifen treatment, IHC with antibodies against selected proteins was performed on tumor tissues arrayed in triplicate on TMAs. Data are represented as mean $\pm$ SEM. * represents $p \leq 0.05$.

(B) Differential protein expression was further analyzed by RPPA. Of the 210 proteins detected by RPPA, only 84 corresponding genes were found to be significantly dysregulated by both adjusted p value and logFC.

(C) The 84 genes were further enriched for gene sets of interest, and the top 12 significantly enriched pathways by the –log10 of the false discovery rate corrected p-value were plotted. These included pathways involved in developmental biology and important signal transduction and signaling cascades.

(D) A correlation heatmap using the 84 differentially expressed proteins and their matched transcriptomics data to understand how well the expression of the genes and proteins correlated with one another.

(E) Heatmap showing a small subset of genes that were positively correlated with their protein expression.

(F) The subset of genes was further enriched for the types of pathways they are heavily involved in. The largest proportion was found to be involved in several signaling pathways including apoptosis and p53 signaling as well as breast cancer hormonal pathways.

(G) A subnetwork exploring the relationship between proteins and transcripts that were differentially expressed (ovals) were used to identify those proteins regulated by TP53 alone (blue), ESR1 alone (red), or co-regulated by both TP53 and ESR1 (purple), which are also known to regulate each other. Differential expression of those genes was assessed (oval outline: blue is downregulated and red is upregulated). See also Table S4.

Changes in the expression of genes regulated by ESR1 (Figure 6G, right panel) included upregulation of the gap junction protein Cx43, consistent with the results of the DEG analysis (Figure 5B). *C6orf211* gene, a transcriptional target of ESR1, which encodes ARMT1 that specifically methylates glutamate side chains of proliferating cell nuclear antigen, which is required for DNA replication and repair, is also upregulated in response to Tam treatment. ARMT1 has been reported to be required for therapeutic susceptibility of luminal breast cancer cells.[37] On the other hand, ATAD2, which binds to ESR1 leading to the upregulation of its target genes including *CCNE1*, *CMYC*, and *E2F1*,[38] is downregulated.

Among the proteins co-regulated by ESR1 and p53 (Figure 6G, center panel) are tumor suppressors, such as SERPINB5 (Maspin) (mammary serine protease), a target of activation by p53,[39] and repression by ESR1.[40] An intriguing finding, consistent with transcriptomic changes determined by RNA sequencing (RNA-seq), is the moderate upregulation of the stem cell markers, SOX9 and ALDH1A in response to Tam therapy. Of the downregulated, co-regulated proteins, CDK1 and BIRC5 (survivin), the latter of which is an inhibitor of apoptosis,[41] are both known pro-oncogenic targets for transcriptional repression by p53. Additionally, we observed transcriptional decreases in MKI67, an important clinical marker of proliferation that is associated with poor prognosis in luminal breast cancer.[42]

Overall, transcriptomic and proteomic-level data revealed Tam treatment, in the context of wild-type p53 in ESR1+ breast cancer patients, altered pathways of intercellular communication, metabolism, DNA repair, proliferation, and stem cell regulation.

DISCUSSION

ESR1 positivity in tumors has been the major guiding eligibility criterion for Tam therapy for breast cancer patients. Although previous retrospective clinical studies have shown that ESR1+ breast tumors with mutant p53[14,15] or with functional p53 deficiency[17] are associated with decreased survival in response to Tam therapy, the molecular mechanisms underlying the impact of Tam on p53 signaling has remained elusive. To gain insight into how Tam affects therapeutically relevant ESR1-p53 crosstalk, we analyzed the effect of Tam on ESR1-p53 interaction and consequential transcriptional and proteomic alterations in treatment-naive patient tumors. Previous prospective presurgical trials with Tam did not include a comprehensive molecular analysis integrating unbiased transcriptomic and proteomic profiling to investigate the functional role of p53 in response to Tam therapy. The clinical study reported here is the only one that addresses the effect of Tam therapy on p53 reactivation by countering the ESR1-p53 interaction. Given that Tam is still the first-line therapy for premenopausal women with ESR1+ breast cancer who are at extremely high risk of recurrence compared to postmenopausal women, a deeper knowledge of early molecular events that occur in response to Tam treatment is required to identify factors and pathways that could be exploited for patient stratification and to develop new strategies to increase therapeutic response. The current study addresses these important issues and provides insights into the early impact of Tam on the crosstalk between ESR1 and wild-type p53, leading to the reactivation of p53.

While the *in situ* PLA data demonstrated disruption of the interaction between ESR1 and p53 in tumors in response to Tam in our randomized trial, analysis of DEGs demonstrated an active p53 regulating multiple target genes. In response to Tam, several transcripts encoding pro-proliferation or anti-apoptotic proteins were downregulated, including those that are components of oncogenic pathways and that are known targets of ESR1. Conversely, various gene transcripts that encode for anti-proliferative proteins were upregulated including those participating in tumor suppressor pathways, which are also targets of p53, ESR1, or both. Consistent with the GSEA analysis, DEGs when enriched by iRegulon revealed the downregulation of several oncogenic MRs, while those associated with tumor suppression and anti-proliferation pathways were upregulated. For example, one of the downregulated MRs, B-Myb (MybL2), is oncogenic and is known to interact with the MuvB core complex (including LIN9, LIN37, LIN52, RBBP4, and LIN54) to form the Myb-MuvB complex, resulting in transcriptional upregulation of genes required for mitosis. The MuvB core interacts with the Rb-like protein p130 and E2F4-DP1 to form the DREAM complex which mediates the global repression of cell cycle genes in G0/G1.[43] In contrast to GSEA in tumors from early breast cancer patients treated with AI for 10–21 days pre-surgery, where cell proliferation and estradiol responses were upregulated in resistant tumors,[44] gene expression in tumors of patients treated with Tam in our trial was diametrically opposite (Figures 5D and 5E). This may reflect a lack of enrichment of resistant tumors in our study or that the pathways involved in resistance to letrozole versus Tam could be different. Consistent with this

observation, the MRs E2F4 and FOXM1 upregulated in the letrozole-resistant patient tumors[44] were downregulated in tumors of patients treated with Tam (Figure S2A).

Furthermore, based on transcriptomic data, our current study suggests that reactivation of p53 by Tam therapy enriches signatures associated with repressed adipogenesis and cholesterol synthesis. As previously noted, one of the most downregulated genes in response to Tam therapy is *DHCR7*, a key enzyme in the mevalonate pathway, which is repressed by the functionally active wild-type p53. Furthermore, p53 blocks the activation of SREBP-2, the master transcriptional regulator of this pathway.[23] This is concordant with the enrichment of JAZF1, a suppressor of SREBP-1[33] (another regulator of cholesterol biosynthesis), as an MR of upregulated genes in response to Tam therapy (Figure S2B). Importantly, squalene epoxidase, a rate-limiting enzyme in cholesterol synthesis and a direct repression target for p53,[45] was downregulated in response to Tam therapy (Figure S2A). Consistent with these observations, our analysis of transcriptional MRs showed that E2F1, which activates the mevalonate pathway,[46] was downregulated in response to Tam treatment (Figure S2A). An increased demand for cholesterol is characteristic of rapidly proliferating cancer cells, which must generate cell membranes and lipid rafts for signaling pathways and transport systems. Cholesterol also serves as the backbone of steroid hormones that can stimulate proliferation and cell growth through the activation of nuclear receptors.[47] Cholesterol-derived oncometabolites such as 25HC and 27HC act as ligands of ESR1 when the activation of ESR1 by endogenous estrogen is blocked by AIs or Tam, and this could be one of the mechanisms of therapeutic resistance.[48] A large prospective trial from Korea showed that higher cholesterol levels are positively associated with breast cancer.[49] Cholesterol is transported by several lipoproteins (LDL and HDL), which may have different effects on cancer risk and progression. Our findings that p53 reactivated by Tam represses cholesterol synthesis pathway unravel a new link between Tam, ESR1, p53, and cholesterol and have important therapeutic implications.

Integration of the transcriptomics data with the proteomics (Figure 6G) provided further insight into the mechanisms underlying the response to Tam therapy. Although several p53-regulated tumor suppressors were upregulated in response to Tam therapy, intriguingly, SOX9, among the genes coregulated by p53 and ESR1, was moderately upregulated in Tam-treated tumors. SOX9 upregulated by RUNX2-ESR1 complex drives resistance to Tam therapy.[50] It controls luminal-to-basal reprogramming and lineage plasticity, is required for expression of the cancer stem cell marker ALDH1, and is elevated in endocrine-resistant breast cancer patient tumors.[51,52] Of note, Tam, besides activating anti-tumorigenic genes, has been reported to activate certain pro-tumorigenic genes in ESR1+ breast tumors although the p53 status in these tumors was not known.[53] A stem cell signature was reported in tumors from relapsing patients compared to Tam-responsive tumors and was also observed very early in breast cancer cells treated with Tam.[54] Consistent with this pattern, basal cell markers KRT5, KRT14, and KRT17 and the stem cell marker ALDH1 were upregulated in our patient cohort in response to Tam therapy. The upregulation of these proteins suggests that there may be a subset of tumor cells resistant to Tam therapy, enabling ESR1 to blunt p53 function. ALDH1+ cells are characteristic of the stem cell population and are known to drive Tam resistance in ESR1+ breast cancer.[55] Whether expression of these markers in Tam-treated patient tumors in the current study reflects the presence of cancer stem cells will need to be analyzed in future studies. If they are cancer stem cells, it would be important to know if this subpopulation existed before Tam therapy, indicating innate resistance, or if they were enriched in response to the therapy, indicating acquired resistance.

Other medications for ESR1+ breast cancer target the ESR1+ breast cancers, including AIs, CDK 4/6 inhibitors, and SERDs. However, these medications have been developed for use in postmenopausal women. We do not know if AIs, SERDS, or CDK 4/6 inhibitors would have a similar impact on the ESR1-p53 interaction. Our findings suggest that Tam and AIs reprogram different gene sets. It is likely that AIs would weaken the interaction between ESR1 and p53 by depleting estrogen; however, AIs may not be as efficient an inhibitor as Tam because, unlike Tam, AIs do not bind ESR1 and change its conformation. This will be an area for future study.

This window-of-opportunity trial is the first to demonstrate that ESR1-p53 crosstalk occurs in patient tumors and that Tam disrupts this interaction, resulting in the functional reactivation of p53. Gene expression in the Tam-treated patient tumors is potentially determined by both the canonical function of Tam as an antagonist of ESR1 and the novel function of Tam as a disruptor of the ESR1-p53 interaction. The presence of this alternative mechanism of action of Tam has significant clinical implications. This study provides valuable input into the importance of a therapeutic strategy based on p53 status-dependent stratification of ESR1+ breast cancer.

Limitations of the study

Our study has some limitations. This study focusing on ESR1+/wild-type p53 breast cancer provided important insight into importance of p53 signaling in response to Tam therapy. Comparing patients with tumors expressing mutant p53 would enhance our findings; however, as expected in the case of ESR1+/HER− breast cancer, patients with tumors expressing mutant p53 were rare in our cohort, making it difficult to compare the two groups. Given that only 20% of ER+ luminal breast cancers harbor mutant p53, it would have been necessary to recruit large number of patients to achieve sufficient statistical power. Because of small number of the patients in the study, there is limitation to the generalization of the results in terms of racial and ethnic diversity of patient population. We lacked paired samples in the treatment and observation arm and therefore could not make direct comparisons of gene and protein expression between the pre-treatment core needle biopsy and the post-treatment surgical specimen from the same individual. There were considerable challenges in retrieving diagnostic samples from other institutions and, in several cases, there was tissue loss during staining of the tissue microarrays. However, unlike other previously published reports that included only patients from the treatment arm, we were able to compare treated and untreated patient samples from surgical specimens that were processed in a similar fashion based on the clinical protocol. Another limitation is the integration of transcriptomics with protein expression data because the number of antibodies in the RPPA is several folds smaller than the 18,000+ transcripts that could be analyzed by RNA-seq. Because of the size heterogeneity of tumors among the patients who completed the trial, we did not have the

same number of tissue specimens for the various assays used in the study. Finally, our study was conducted between 2009 and 2015. We recognize that treatment guidelines for ER+/HER− breast cancer have evolved since then. However, Tam remains the first-line adjuvant treatment for premenopausal women with early-stage, low-risk ER+/HER− breast cancer.[8]

STAR★METHODS

Detailed methods are provided in the online version of this paper and include the following:

- KEY RESOURCES TABLE
- RESOURCE AVAILABILITY
  - Lead contact
  - Materials availability
  - Data and code availability
- EXPERIMENTAL MODEL AND STUDY PARTICIPANT DETAILS
  - Patient population and study design
- METHOD DETAILS
  - Collection of tumor tissue
  - Collection of blood specimens
  - Analysis of tamoxifen and metabolites
  - Population pharmacokinetic (PK) modeling
  - Genotyping
  - Determination of p53 status in tumor samples
  - Immunohistochemical staining and scoring of the human breast cancer tissue micro array (TMA)
  - Proximity ligation assay (PLA)
  - RNA-seq and gene expression analysis
  - Reverse phase protein array (RPPA)
- QUANTIFICATION AND STATISTICAL ANALYSIS
  - Statistical methods

SUPPLEMENTAL INFORMATION

Supplemental information can be found online at https://doi.org/10.1016/j.isci.2024.109995.

AUTHOR CONTRIBUTIONS

Conceptualization, G.M.D. and S. Kulkarni; investigation and methodology, G.M.D., S. Kulkarni, C.C.O., S.R.R., A.D.H., A.G., S.B.E., W.M.S., J.W., J.H.P., B.A.K., P.K.S., S. Kumar, H.H.C., M.R., A.A., M.G., and A.K.L.G.; resources, G.M.D., S. Kulkarni, S.B.E., S. Kumar, H.H.C., P.K.S., A.D.H., C.D.M., A.A., and A.K.L.G.; writing – original draft, G.M.D., S. Kulkarni, C.C.O., and S.R.R.; writing – review and editing, G.M.D., S. Kulkarni, S.R.R., C.C.O., W.M.S., M.G., and A.K.L.G.; visualization, G.M.D., S. Kulkarni, C.C.O., S.R.R., A.G., A.A., and M.G.; supervision, G.M.D. and S. Kulkarni; project administration, G.M.D. and S. Kulkarni; funding acquisition, G.M.D. and S. Kulkarni.

DECLARATION OF INTERESTS

The authors declare no competing interests.

REFERENCES

1. Heer, E., Harper, A., Escandor, N., Sung, H., McCormack, V., and Fidler-Benaoudia, M.M. (2020). Global burden and trends in premenopausal and postmenopausal breast cancer: a population-based study. Lancet Global Health 8, e1027–e1037. https://doi.org/10.1016/S2214-109X(20)30215-1.

2. Jensen, E.V., and Jordan, V.C. (2003). The estrogen receptor: a model for molecular medicine. Clin. Cancer Res. 9, 1980–1989.

3. Howell, A., and Howell, S.J. (2023). Tamoxifen evolution. Br. J. Cancer 128, 421–425. https://doi.org/10.1038/s41416-023-02158-5.

4. Group, E.B.C.T.C. (1998). Tamoxifen for early breast cancer: an overview of the randomised trials. Early Breast Cancer Trialists' Collaborative Group. Lancet 351, 1451–1467.

5. Davies, C., Pan, H., Godwin, J., Gray, R., Arriagada, R., Raina, V., Abraham, M., Medeiros Alencar, V.H., Badran, A., Bonfill, X., et al. (2013). Long-term effects of continuing adjuvant tamoxifen to 10 years versus stopping at 5 years after diagnosis of oestrogen receptor-positive breast cancer: ATLAS, a randomised trial. Lancet 381, 805–816. https://doi.org/10.1016/S0140-6736(12)61963-1.

6. Fisher, B., Costantino, J.P., Wickerham, D.L., Redmond, C.K., Kavanah, M., Cronin, W.M., Vogel, V., Robidoux, A., Dimitrov, N., Atkins, J., et al. (1998). Tamoxifen for prevention of breast cancer: report of the National Surgical Adjuvant Breast and Bowel Project P-1 Study. J. Natl. Cancer Inst. 90, 1371–1388.

7. Waks, A.G., and Winer, E.P. (2019). Breast Cancer Treatment: A Review. JAMA 321, 288–300. https://doi.org/10.1001/jama.2018.19323.

8. (2023). National Copmprehensive Cancer Network. (2023). NCCN Guidelines® Insights: Breast Cancer, Version. J. Natl. Compr. Canc. Netw. 21, 594–608. https://doi.org/10.6004/jnccn.2023.0031.

9. Kastenhuber, E.R., and Lowe, S.W. (2017). Putting p53 in Context. Cell 170, 1062–1078. https://doi.org/10.1016/j.cell.2017.08.028.

10. Vousden, K.H., and Prives, C. (2009). Blinded by the Light: The Growing Complexity of p53. Cell 137, 413–431. https://doi.org/10.1016/j.cell.2009.04.037.

11. Liu, W., Konduri, S.D., Bansal, S., Nayak, B.K., Rajasekaran, S.A., Karuppayil, S.M., Rajasekaran, A.K., and Das, G.M. (2006). Estrogen receptor-alpha binds p53 tumor suppressor protein directly and represses its function. J. Biol. Chem. 281, 9837–9840.

12. Liu, W., Ip, M.M., Podgorsak, M.B., and Das, G.M. (2009). Disruption of estrogen receptor alpha-p53 interaction in breast tumors: a novel mechanism underlying the anti-tumor effect of radiation therapy. Breast Cancer Res. Treat. 115, 43–50. https://doi.org/10.1007/s10549-008-0044-z.

13. Konduri, S.D., Medisetty, R., Liu, W., Kaipparettu, B.A., Srivastava, P., Brauch, H., Fritz, P., Swetzig, W.M., Gardner, A.E., Khan, S.A., and Das, G.M. (2010). Mechanisms of estrogen receptor antagonism toward p53 and its implications in breast cancer therapeutic response and stem cell regulation. Proc. Natl. Acad. Sci. USA 107, 15081–15086. https://doi.org/10.1073/pnas.1009575107.

14. Bergh, J., Norberg, T., Sjögren, S., Lindgren, A., and Holmberg, L. (1995). Complete sequencing of the p53 gene provides prognostic information in breast cancer patients, particularly in relation to adjuvant systemic therapy and radiotherapy. Nat. Med. 1, 1029–1034.

15. Berns, E.M., Foekens, J.A., Vossen, R., Look, M.P., Devilee, P., Henzen-Logmans, S.C., van Staveren, I.L., van Putten, W.L., Inganäs, M., Meijer-van Gelder, M.E., et al. (2000). Complete sequencing of TP53 predicts poor response to systemic therapy of advanced breast cancer. Cancer Res. 60, 2155–2162.

16. Coates, A.S., Millar, E.K.A., O'Toole, S.A., Molloy, T.J., Viale, G., Goldhirsch, A., Regan, M.M., Gelber, R.D., Sun, Z., Castiglione-Gertsch, M., et al. (2012). Prognostic interaction between expression of p53 and estrogen receptor in patients with node-negative breast cancer: results from IBCSG Trials VIII and IX. Breast Cancer Res. 14, R143. https://doi.org/10.1186/bcr3348.

17. Miller, L.D., Smeds, J., George, J., Vega, V.B., Vergara, L., Ploner, A., Pawitan, Y., Hall, P., Klaar, S., Liu, E.T., and Bergh, J. (2005). An expression signature for p53 status in human breast cancer predicts mutation status, transcriptional effects, and patient survival. Proc. Natl. Acad. Sci. USA 102, 13550–13555.

18. Kisanga, E.R., Gjerde, J., Guerrieri-Gonzaga, A., Pigatto, F., Pesci-Feltri, A., Robertson, C., Serrano, D., Pelosi, G., Decensi, A., and Lien, E.A. (2004). Tamoxifen and metabolite concentrations in serum and breast cancer tissue during three dose regimens in a randomized preoperative trial. Clin. Cancer Res. 10, 2336–2343. https://doi.org/10.1158/1078-0432.ccr-03-0538.

19. Klein, D.J., Thorn, C.F., Desta, Z., Flockhart, D.A., Altman, R.B., and Klein, T.E. (2013). PharmGKB summary: tamoxifen pathway, pharmacokinetics. Pharmacogenetics Genom. 23, 643–647. https://doi.org/10.1097/FPC.0b013e3283656bc1.

20. Marcath, L.A., Deal, A.M., Van Wieren, E., Danko, W., Walko, C.M., Ibrahim, J.G., Weck, K.E., Jones, D.R., Desta, Z., McLeod, H.L., et al. (2017). Comprehensive assessment of cytochromes P450 and transporter genetics with endoxifen concentration during tamoxifen treatment. Pharmacogenetics Genom. 27, 402–409. https://doi.org/10.1097/FPC.0000000000000311.

21. ter Heine, R., Binkhorst, L., de Graan, A.J.M., de Bruijn, P., Beijnen, J.H., Mathijssen, R.H.J., and Huitema, A.D.R. (2014). Population pharmacokinetic modelling to assess the impact of CYP2D6 and CYP3A metabolic phenotypes on the pharmacokinetics of tamoxifen and endoxifen. Br. J. Clin. Pharmacol. 78, 572–586. https://doi.org/10.1111/bcp.12388.

22. Puszkiel, A., Arellano, C., Vachoux, C., Evrard, A., Le Morvan, V., Boyer, J.C., Robert, J., Delmas, C., Dalenc, F., Debled, M., et al. (2021). Model-Based Quantification of Impact of Genetic Polymorphisms and Co-Medications on Pharmacokinetics of Tamoxifen and Six Metabolites in Breast Cancer. Clin. Pharmacol. Ther. 109, 1244–1255. https://doi.org/10.1002/cpt.2077.

23. Moon, S.H., Huang, C.H., Houlihan, S.L., Regunath, K., Freed-Pastor, W.A., Morris, J.P., 4th, Tschaharganeh, D.F., Kastenhuber, E.R., Barsotti, A.M., Culp-Hill, R., et al. (2019). p53 Represses the Mevalonate Pathway to Mediate Tumor Suppression. Cell 176, 564–580.e19. https://doi.org/10.1016/j.cell.2018.11.011.

24. Aasen, T., Leithe, E., Graham, S.V., Kameritsch, P., Mayán, M.D., Mesnil, M., Pogoda, K., and Tabernero, A. (2019). Connexins in cancer: bridging the gap to the clinic. Oncogene 38, 4429–4451. https://doi.org/10.1038/s41388-019-0741-6.

25. Janky, R., Verfaillie, A., Imrichová, H., Van de Sande, B., Standaert, L., Christiaens, V., Hulselmans, G., Herten, K., Naval Sanchez, M., Potier, D., et al. (2014). iRegulon: from a gene list to a gene regulatory network using large motif and track collections. PLoS Comput. Biol. 10, e1003731. https://doi.org/10.1371/journal.pcbi.1003731.

26. Khaleel, S.S., Andrews, E.H., Ung, M., DiRenzo, J., and Cheng, C. (2014). E2F4 regulatory program predicts patient survival prognosis in breast cancer. Breast Cancer Res. 16, 486. https://doi.org/10.1186/s13058-014-0486-7.

27. Miller, T.W., Balko, J.M., Fox, E.M., Ghazoui, Z., Dunbier, A., Anderson, H., Dowsett, M., Jiang, A., Smith, R.A., Maira, S.M., et al. (2011). ERalpha-dependent E2F transcription can mediate resistance to estrogen deprivation in human breast cancer. Cancer Discov. 1, 338–351. https://doi.org/10.1158/2159-8290.CD-11-0101.

28. Zhang, Y.L., Ma, Y., Zeng, Y.Q., Liu, Y., He, E.P., Liu, Y.T., Qiao, F.L., Yu, R., Wang, Y.S., Wu, X.Y., and Leng, P. (2021). A narrative review of research progress on FoxM1 in breast cancer carcinogenesis and therapeutics. Ann. Transl. Med. 9, 1704. https://doi.org/10.21037/atm-21-5271.

29. Barsotti, A.M., and Prives, C. (2009). Pro-proliferative FoxM1 is a target of p53-mediated repression. Oncogene 28, 4295–4305. https://doi.org/10.1038/onc.2009.282.

30. Pandit, B., Halasi, M., and Gartel, A.L. (2009). p53 negatively regulates expression of FoxM1. Cell Cycle 8, 3425–3427.

31. Bayley, R., Ward, C., and Garcia, P. (2020). MYBL2 amplification in breast cancer: Molecular mechanisms and therapeutic potential. Biochim. Biophys. Acta Rev. Canc 1874, 188407. https://doi.org/10.1016/j.bbcan.2020.188407.

32. Sekiya, M., Kainoh, K., Sugasawa, T., Yoshino, R., Hirokawa, T., Tokiwa, H., Nakano, S., Nagatoishi, S., Tsumoto, K., Takeuchi, Y., et al. (2021). The transcriptional corepressor CtBP2 serves as a metabolite sensor orchestrating hepatic glucose and lipid

homeostasis. Nat. Commun. *12*, 6315. https://doi.org/10.1038/s41467-021-26638-5.

33. Wei, Q., Zhou, B., Yang, G., Hu, W., Zhang, L., Liu, R., Li, M., Wang, K., Gu, H.F., Guan, Y., et al. (2018). JAZF1 ameliorates age and diet-associated hepatic steatosis through SREBP-1c -dependent mechanism. Cell Death Dis. *9*, 859. https://doi.org/10.1038/s41419-018-0923-0.

34. Hoxhaj, G., and Manning, B.D. (2020). The PI3K-AKT network at the interface of oncogenic signalling and cancer metabolism. Nat. Rev. Cancer *20*, 74–88. https://doi.org/10.1038/s41568-019-0216-7.

35. Szklarczyk, D., Gable, A.L., Lyon, D., Junge, A., Wyder, S., Huerta-Cepas, J., Simonovic, M., Doncheva, N.T., Morris, J.H., Bork, P., et al. (2019). STRING v11: protein-protein association networks with increased coverage, supporting functional discovery in genome-wide experimental datasets. Nucleic Acids Res. *47*, D607–D613. https://doi.org/10.1093/nar/gky1131.

36. Bajaj, S., Alam, S.K., Roy, K.S., Datta, A., Nath, S., and Roychoudhury, S. (2016). E2 Ubiquitin-conjugating Enzyme, UBE2C Gene, Is Reciprocally Regulated by Wild-type and Gain-of-Function Mutant p53. J. Biol. Chem. *291*, 14231–14247. https://doi.org/10.1074/jbc.M116.731398.

37. Perry, J.J.P., Ballard, G.D., Albert, A.E., Dobrolecki, L.E., Malkas, L.H., and Hoelz, D.J. (2015). Human C6orf211 encodes Armt1, a protein carboxyl methyltransferase that targets PCNA and is linked to the DNA damage response. Cell Rep. *10*, 1288–1296. https://doi.org/10.1016/j.celrep.2015.01.054.

38. Caron, C., Lestrat, C., Marsal, S., Escoffier, E., Curtet, S., Virolle, V., Barbry, P., Debernardi, A., Brambilla, C., Brambilla, E., et al. (2010). Functional characterization of ATAD2 as a new cancer/testis factor and a predictor of poor prognosis in breast and lung cancers. Oncogene *29*, 5171–5181. https://doi.org/10.1038/onc.2010.259.

39. Zou, Z., Gao, C., Nagaich, A.K., Connell, T., Saito, S., Moul, J.W., Seth, P., Appella, E., and Srivastava, S. (2000). p53 regulates the expression of the tumor suppressor gene maspin. J. Biol. Chem. *275*, 6051–6054. https://doi.org/10.1074/jbc.275.9.6051.

40. Liu, Z., Shi, H.Y., Nawaz, Z., and Zhang, M. (2004). Tamoxifen induces the expression of maspin through estrogen receptor-alpha. Cancer Lett. *209*, 55–65. https://doi.org/10.1016/j.canlet.2003.11.018.

41. Hoffman, W.H., Biade, S., Zilfou, J.T., Chen, J., and Murphy, M. (2002). Transcriptional repression of the anti-apoptotic survivin gene by wild type p53. J. Biol. Chem. *277*, 3247–3257.

42. Zhang, A., Wang, X., Fan, C., and Mao, X. (2021). The Role of Ki67 in Evaluating Neoadjuvant Endocrine Therapy of Hormone Receptor-Positive Breast Cancer. Front. Endocrinol. *12*, 687244. https://doi.org/10.3389/fendo.2021.687244.

43. Iness, A.N., Felthousen, J., Ananthapadmanabhan, V., Sesay, F., Saini, S., Guiley, K.Z., Rubin, S.M., Dozmorov, M., and Litovchick, L. (2019). The cell cycle regulatory DREAM complex is disrupted by high expression of oncogenic B-Myb. Oncogene *38*, 1080–1092. https://doi.org/10.1038/s41388-018-0490-y.

44. Giltnane, J.M., Hutchinson, K.E., Stricker, T.P., Formisano, L., Young, C.D., Estrada, M.V., Nixon, M.J., Du, L., Sanchez, V., Ericsson, P.G., et al. (2017). Genomic profiling of ER(+) breast cancers after short-term estrogen suppression reveals alterations associated with endocrine resistance. Sci. Transl. Med. *9*, eaai7993. https://doi.org/10.1126/scitranslmed.aai7993.

45. Sun, H., Li, L., Li, W., Yang, F., Zhang, Z., Liu, Z., and Du, W. (2021). p53 transcriptionally regulates SQLE to repress cholesterol synthesis and tumor growth. EMBO Rep. *22*, e52537. https://doi.org/10.15252/embr.202152537.

46. Shamma, A., Takegami, Y., Miki, T., Kitajima, S., Noda, M., Obara, T., Okamoto, T., and Takahashi, C. (2009). Rb Regulates DNA damage response and cellular senescence through E2F-dependent suppression of N-ras isoprenylation. Cancer Cell *15*, 255–269. https://doi.org/10.1016/j.ccr.2009.03.001.

47. Guerra, B., Recio, C., Aranda-Tavío, H., Guerra-Rodríguez, M., García-Castellano, J.M., and Fernández-Pérez, L. (2021). The Mevalonate Pathway, a Metabolic Target in Cancer Therapy. Front. Oncol. *11*, 626971. https://doi.org/10.3389/fonc.2021.626971.

48. Nelson, E.R., Chang, C.Y., and McDonnell, D.P. (2014). Cholesterol and breast cancer pathophysiology. Trends Endocrinol. Metab. *25*, 649–655. https://doi.org/10.1016/j.tem.2014.10.001.

49. Kitahara, C.M., Berrington de González, A., Freedman, N.D., Huxley, R., Mok, Y., Jee, S.H., and Samet, J.M. (2011). Total cholesterol and cancer risk in a large prospective study in Korea. J. Clin. Oncol. *29*, 1592–1598. https://doi.org/10.1200/JCO.2010.31.5200.

50. Jeselsohn, R., Cornwell, M., Pun, M., Buchwalter, G., Nguyen, M., Bango, C., Huang, Y., Kuang, Y., Paweletz, C., Fu, X., et al. (2017). Embryonic transcription factor SOX9 drives breast cancer endocrine resistance. Proc. Natl. Acad. Sci. USA *114*, E4482–E4491. https://doi.org/10.1073/pnas.1620993114.

51. Domenici, G., Aurrekoetxea-Rodríguez, I., Simões, B.M., Rábano, M., Lee, S.Y., Millán, J.S., Comaills, V., Oliemuller, E., López-Ruiz, J.A., Zabalza, I., et al. (2019). A Sox2-Sox9 signalling axis maintains human breast luminal progenitor and breast cancer stem cells. Oncogene *38*, 3151–3169. https://doi.org/10.1038/s41388-018-0656-7.

52. Christin, J.R., Wang, C., Chung, C.Y., Liu, Y., Dravis, C., Tang, W., Oktay, M.H., Wahl, G.M., and Guo, W. (2020). Stem Cell Determinant SOX9 Promotes Lineage Plasticity and Progression in Basal-like Breast Cancer. Cell Rep. *31*, 107742. https://doi.org/10.1016/j.celrep.2020.107742.

53. Frasor, J., Chang, E.C., Komm, B., Lin, C.Y., Vega, V.B., Liu, E.T., Miller, L.D., Smeds, J., Bergh, J., and Katzenellenbogen, B.S. (2006). Gene expression preferentially regulated by tamoxifen in breast cancer cells and correlations with clinical outcome. Cancer Res. *66*, 7334–7340. https://doi.org/10.1158/0008-5472.CAN-05-4269.

54. Notas, G., Pelekanou, V., Kampa, M., Alexakis, K., Sfakianakis, S., Laliotis, A., Askoxilakis, J., Tsentelierou, E., Tzardi, M., Tsapis, A., and Castanas, E. (2015). Tamoxifen induces a pluripotency signature in breast cancer cells and human tumors. Mol. Oncol. *9*, 1744–1759. https://doi.org/10.1016/j.molonc.2015.05.008.

55. Simoes, B.M., O'Brien, C.S., Eyre, R., Silva, A., Yu, L., Sarmiento-Castro, A., Alferez, D.G., Spence, K., Santiago-Gomez, A., Chemi, F., et al. (2015). Anti-estrogen Resistance in Human Breast Tumors Is Driven by JAG1-NOTCH4-Dependent Cancer Stem Cell Activity. Cell Rep. *12*, 1968–1977. https://doi.org/10.1016/j.celrep.2015.08.050.

56. Kwa, M., Makris, A., and Esteva, F.J. (2017). Clinical utility of gene-expression signatures in early stage breast cancer. Nat. Rev. Clin. Oncol. *14*, 595–610. https://doi.org/10.1038/nrclinonc.2017.74.

57. Paik, S., Shak, S., Tang, G., Kim, C., Baker, J., Cronin, M., Baehner, F.L., Walker, M.G., Watson, D., Park, T., et al. (2004). A multigene assay to predict recurrence of tamoxifen-treated, node-negative breast cancer. N. Engl. J. Med. *351*, 2817–2826. https://doi.org/10.1056/NEJMoa041588.

58. U.S. Department of Health and Human Services. F.a.D (2001). Administration, editor. Guidance for Industry. In Bioanalytical Method Validation (U.S. Department of Health and Human Services Food and Drug Administration).

59. Wilton, J., Kurenova, E., Pitzonka, L., Gaudy, A., Curtin, L., Sexton, S., Cance, W., and Fetterly, G. (2016). Pharmacokinetic analysis of the FAK scaffold inhibitor C4 in dogs. Eur. J. Drug Metab. Pharmacokinet. *41*, 55–67. https://doi.org/10.1007/s13318-014-0233-6.

60. Adjei, A.A., Mandrekar, S.J., Dy, G.K., Molina, J.R., Adjei, A.A., Gandara, D.R., Ziegler, K.L.A., Stella, P.J., Rowland, K.M., Jr., Schild, S.E., and Zinner, R.G. (2010). Phase II trial of pemetrexed plus bevacizumab for second-line therapy of patients with advanced non-small-cell lung cancer: NCCTG and SWOG study N0426. J. Clin. Oncol. *28*, 614–619. https://doi.org/10.1200/JCO.2009.23.6406.

61. Coarfa, C., Grimm, S.L., Rajapakshe, K., Perera, D., Lu, H.Y., Wang, X., Christensen, K.R., Mo, Q., Edwards, D.P., and Huang, S. (2021). Reverse-Phase Protein Array: Technology, Application, Data Processing, and Integration. J. Biomol. Tech. *32*, 15–29. https://doi.org/10.7171/jbt.21-3202-001.

62. Bu, W., Liu, Z., Jiang, W., Nagi, C., Huang, S., Edwards, D.P., Jo, E., Mo, Q., Creighton, C.J., Hilsenbeck, S.G., et al. (2019). Mammary Precancerous Stem and Non-Stem Cells Evolve into Cancers of Distinct Subtypes. Cancer Res. *79*, 61–71. https://doi.org/10.1158/0008-5472.CAN-18-1087.

STAR★METHODS

KEY RESOURCES TABLE

REAGENT or RESOURCE	SOURCE	IDENTIFIER
Antibodies		
ER alpha/ESR1	Santa Cruz Biotechnology	Cat#sc-543; RRID: AB_631471
p53	Santa Cruz Biotechnology	Cat#sc-126; RRID: AB_628082
p21	Agilent	Cat#M7202; RRID: AB_2077700
MDM2	Millipore	Cat#OP46; RRID: AB_564803
Chemicals, peptides, and recombinant proteins		
Tamoxifen	Mylan Pharmaceuticals Inc.	NDC 0378-0274-93
N-desmethyltamoxifen	Millipore-Sigma	Cat# D9069
(E/Z)-endoxifen	Millipore-Sigma	Cat# E8284
(Z)-4-hydroxytamoxifen	Millipore-Sigma	Cat# H6278
Z)-4-hydroxytamoxifen-d_5	Toronto Research Chemicals	Cat# TRC-H954771
α-hydroxytamoxifen	Toronto Research Chemicals	Cat# TRC-H954710
4'-hydroxytamoxifen	Toronto Research Chemicals	Cat# TRC-H954730
Methanol	Millipore-Sigma	Cat# 34860
Acetonitrile	Millipore-Sigma	Cat# 34851
AMPure XP SPRI Reagent	Beckman Coulter	Cat# A63881
TruSeq Custom Amplicon kit	Illumina Inc.	Cat# 20005718
Dako EnVision®+ Dual Link System-HRP	Agilent Technologies, Inc.	Cat# K4065
ProLong™ Gold Antifade Mountant	Thermo Fisher Scientific	Cat# P36934
Phenomenex Kinetex C18 column	Phenomenex, Torrance	Cat# 00B-4462-AN
Krudkatcher in-line filter	Phenomenex, Torrance	Cat# AF0-8497
TruSeq Stranded Total RNA kit	Illumina Inc.	Cat# 15032618
Duolink® *In Situ* Detection Reagents Brightfield	Millipore-Sigma	Cat# DUO92012
MiSeq Reagent Kits v2	Illumina Inc.	Cat# MS-102-2002
All prep DNA/RNA/Protein kit	QIAGEN	Cat# 80004
DNase digestion using DNase I	Thermo Fisher Scientific	Cat# 18068015
TruSeq Custom Amplicon kit	Illumina Inc.	Cat# 20005718
AmpureXP beads	Beckman Coulter	Cat# A63881
KAPA Biosystems qPCR kit v2	Roche Diagnostics Corporation	Cat# KK4873
Alkaline phosphatase	Sequenom	Cat# 001107
Flex Target Retrieval Solution High pH	Agilent Technologies, Inc.	Cat# GV804
Flex Target Retrieval Solution Low pH	Agilent Technologies, Inc.	Cat# GV805
Flex HRP polymer	Agilent Technologies, Inc.	Cat# DM843
HRP	Agilent Technologies, Inc.	GV823
DAB	Agilent Technologies, Inc.	CAT# K3468
Peroxidase-Blocking Reagent	Agilent Technologies, Inc.	Cat# GV823
DAB (Diaminobenzidine)	Agilent Technologies, Inc.	Cat# K3468
Duolink® *In Situ* Detection Reagents Brightfield Box A	Millipore-Sigma	Cat# DUO92012A

Continued

REAGENT or RESOURCE	SOURCE	IDENTIFIER
Duolink® *In Situ* Detection Reagents Brightfield Box B	Millipore-Sigma	Cat# DUO92012B
Epredia™ ClearVue™ Mountants	Fisher Scientific	Cat# 23425401
DNase digestion using DNase I	Invitrogen	Cat# 18068015
4200 Tape Station D1000 Screentape	Agilent Technologies, Inc.	Part No# 5067-5582
Beta-Mercaptoethanol	Millipore-Sigma	Cat# M6250
T-PER™ Tissue Protein Extraction Reagent	Thermo Fisher Scientific	Cat# 78510
cOmplete™, EDTA-free Protease Inhibitor	Roche® Life Science	Cat# 11873580001
IRDye® 680RD Streptavidin	LI-COR Biosciences	Cat# 926-68079
SYPRO™ Ruby Protein Blot Stain	Thermo Fisher Scientific	Cat# S11791
Critical commercial assays		
Duolink® *In Situ* Detection Reagents Brightfield PLA	Millipore-Sigma	Cat# DUO92012
Pierce™ BCA Protein Assay Kits	Thermo Fisher Scientific	Cat# 23225
Clearify	American Mastertech	Cat# CACLEGAL
Mass ARRAY Compact system	Sequenom	Sequenom
Deposited data		
Data deposition in GEO. GEO accession GSE263089		https://secure-web.cisco.com/10bsvp2vPmQYSjAKYlCuFZlsc-EKtf_3r9Y4he-X3ggQDC0YclZrJ2wRCr9VZHVbrLDilwJOdbd BpVl8dlLmZTj4TKLprgSnqWrU-UBc1lMcu4W4byVePlz9HKZ ua1r2POAKCyFc-TYJErcfKLShDJl4LlPbubnw3Dai0LasW_ sT2ZQBrDsM6zLZf8XNcCA89SH69sylgJpNpcREmvaxr EM4cvPQZj0xXheqWqTwazYQ0tg3N9TckPIMoeBD- d6IHVeFZliROlsy94brkidlVsbmhtBsB9E-EiHXrdzwvM- C9uP6YjJzuayOaLDEIIE-T/https%3A%2F%2F www.ncbi.nlm.nih.gov%2Fgeo%2Fquery%2 Facc.cgi%3Facc%3DGSE263089 Token-exedcgiqbfwrxcv
Software and algorithms		
NONMEM 7.4.1	ICON Development Solutions	https://www.iconplc.com/
Pirana 2.9.7		pirana-software.com
Coriell Cell Repository		http://ccr.coriell.org
iRegulon (Vsn 1.3)	iRegulon	http://iregulon.aertslab.org/download.html
Illumina Design Studio Software	Illumina	https://www.illumina.com/products/by-type/ informatics-products/designstudio.html
Prism (Version 9)	GraphPad	https://www.graphpad.com/features
Cytoscape Network and Visualization Application (Vsn 2.8.x)	Cytoscope	https://cytoscape.org/
GenePix Pro 7.0	Molecular Devices	https://support.moleculardevices.com
STRING-db algorithm	STRING	https://string-db.org
DESeq2' Vsn 1.30	Bioconductor	https://www.bioconductor.org
Molecular Signatures Database (MSigDB)	GSEA	https://www.gsea-msigdb.org/gsea/msigdb/
Enriched Volcano (Vsn 1.11.3)	CRAN	https://cran.r-project.org
corrplot (Vsn 0.92)	CRAN	https://cran.r-project.org
gplots' (Vsn 3.1.3.1)	CRAN	https://cran.r-project.org
clusterProfiler' (Vsn 3.0.4)	Bioconductor	https://www.bioconductor.org
limma' (Vsn 3.2.0)	Bioconductor	http://bioconductor.org

Continued

REAGENT or RESOURCE	SOURCE	IDENTIFIER
gplots' (Vsn 3.1.3.1)	CRAN	https://cran.r-project.org
R Statistical Software (Vsn. 3.4.1).	CRAN	https://cran.r-project.org
Other		
RNA quantification	NanoDrop™ 8000 Spectrophotometer	Cat# ND-8000-GL
BondRX Auto stainer for Immunohistochemistry	Leica Biosystems	Cat# 21.2821

RESOURCE AVAILABILITY

Lead contact

Further information and requests for resources and reagents should be directed to and will be fulfilled by the lead contact, Dr. Gokul M. Das (gokul.das@roswellpark.org).

Materials availability

This study did not generate new unique reagents.

Data and code availability

- RNA-seq data have been deposited at Gene Expression Omnibus (GEO) and are publicly available as of the date of publication. Accession number is listed in the key resources table.
- This paper does not report original code.
- Any additional information required to reanalyze the data reported in this paper is available from the lead contact upon request.

EXPERIMENTAL MODEL AND STUDY PARTICIPANT DETAILS

Patient population and study design

This clinical trial was designed as a randomized window of opportunity pilot trial (NCT01027416) of Tam versus no intervention control (standard of care), employing a blocked randomization scheme and stratified by clinical site. After appropriate institutional regulatory approvals (Institutional Review Board ID: I-110907), recruitment began in 2010 and was completed in 2015. Pre and postmenopausal patients were recruited from two institutions: the Roswell Park Comprehensive Cancer Center and the University of Chicago Medical School. The following patients were approached for participation: those with a diagnosis of ESR1+ invasive breast cancer on a core needle biopsy, with a mass greater than 1 cm on mammography, ultrasound, or MRI, who were planning for surgical excision of the tumor as their initial therapy. After informed consent was obtained, participants were randomized to Arm 1: standard of care, which meant that patients underwent surgical intervention at the next available surgical date per standard of care or Arm 2: 20 mg of Tam by mouth once daily for 28 days immediately preceding surgical therapy (See Figure 1). All patients who met the following eligibility criteria were included: all participants had to have an ECOG score of 0 or 1. Women with inoperable tumors or stage 4 disease, pregnant or lactating women and women who had received prior therapy for breast cancer, including irradiation, chemotherapy, immunotherapy, and/or hormonal therapy, were ineligible. Patients who had received postmenopausal hormonal replacement therapy, infertility medications, Tam, raloxifene, AIs, and/or herbal supplements 30 days before their diagnostic biopsy were not eligible. Women taking oral contraceptives were permitted as long as they did not start or stop the medication while on Tam. Patients with known or suspected hypercoagulable syndrome or a history of venous or arterial thrombosis were excluded. Finally, patients with a known mutation in p53 (Li Fraumeni Syndrome) were ineligible. Unevaluable patients were defined as participants who did not have sufficient tissue for the study or who did not complete the intervention and were replaced in the study. Enrollment in the study was predicated on the presence of ESR1, based on an Allred score of 3 or above. Data on progesterone receptor (PR) expression were collected but were not used as an eligibility criterion. Human epidermal growth factor receptor 2 (HER2) expression status was not required prior to accrual, but patients who were HER-2 positive were referred for neoadjuvant chemotherapy and were not enrolled. Finally, Oncotype DX scores[56,57] were collected from patients who underwent testing after surgery. Representativeness of study participants are shown in Table S1. Number of patients enrolled and completed the study at the two participating institutions are listed in Table S2. Details of participant profiles are in Table S3. The patient population consists of only women because breast cancer mainly affects women. It is unclear if the observations in women patients will be generalizable to men with breast cancer.

METHOD DETAILS

Collection of tumor tissue

After standard-of-care surgery for breast cancer, the tumor tissue was immediately transported on ice to the pathology gross room. Fresh tumor tissues were snap frozen for analysis with in 60 min of surgical excision. All tissue procurement activities for the patients enrolled in

the study were directed and recorded by the Laboratory Information Management System (LIMS) in a HIPPA-compliant manner. The system also tracks the life history of a biospecimen through its procurement, storage, and distribution along with all associated core laboratory data.

Collection of blood specimens

Two tubes of blood (10 mL each), were drawn 0–30 days prior to the first dose of Tam for pharmacokinetic analysis and genotyping of *CYP2D6* and *CYP3A4/5* variants, and additional pharmacokinetic samples of one tube 3–6 h post dose for those patients receiving Tam in the morning or one tube at 12 ± 4 h prior to the next day's dose for those patients receiving Tam in the evening in weeks 2, 3, or 4. An additional pharmacokinetic sample was collected at 24 h ± 12 h for all patients on the morning of the surgery. Patients were asked to stop their Tam the day before surgery; therefore, those taking Tam at night took their last dose at 36 h prior to surgery, and those taking Tam in the morning would be taking their last dose approximately 24 h before surgery. Blood drawn prior to Tam administration was used to determine the genotype of *CYP2D6* and *CYP3A4/5* and to ensure that the Tam levels were zero.

Analysis of tamoxifen and metabolites

Tamoxifen and its metabolites in the plasma and breast tissue samples were analyzed using a validated LC-MS/MS assay, following FDA guidance,[58] for (Z)-tamoxifen ((Z)-TAM) and the following metabolites: (Z)-N-desmethyltamoxifen ((Z)-ND-TAM), (Z)-4-endoxifen ((Z)-END), and (Z)-4-hydroxytamoxifen ((Z)-4-OH-TAM). Plasma and homogenized breast tissue samples (50 μL) were prepared using an acetonitrile protein precipitation extraction procedure where the acetonitrile contained 4-hydroxytamoxifen-d_5 and tamoxifen-d_5 as internal standards. LC-MS/MS analysis of the extracted samples was performed using a Shimadzu (Kyoto, Japan) high pressure liquid chromatographic (HPLC) system and a 5500 mass spectrometer (Sciex, Framingham, MA) with electrospray ionization (ESI). For tamoxifen and metabolites, chromatographic separation was achieved using a biphasic gradient over a Phenomenex Kinetex C18 column (2.1 × 50 mm, Phenomenex, Torrance, California) preceded by a Krudkatcher in-line filter (Phenomenex). The extracts were injected for analysis into the LC-MS/MS analytical system and the analytes quantitated over the following calibration ranges: 1.00–400 ng/mL for TAM and ND-TAM, 0.500–200 ng/mL for END and 0.250–100 ng/mL for 4-OH-TAM. In addition to TAM and these three metabolites, α-hydroxytamoxifen, (Z)-4'-hydroxytamoxifen ((Z)-4'-OH-TAM), and (Z)-4'-endoxifen ((Z)-4'-END) were obtained and chromatographed to ensure selectivity for the validated analytes. (Z) and (E) isomers were also chromatographically separated and (Z)-tamoxifen-N-oxide (TAM-N-Oxide) was monitored virtually based on theoretical Q1/Q3 masses.[59] (Z)-TAM, (Z)-ND-TAM, (Z)-END, (Z)-4-OH-TAM were all back-calculated using calibration curves constructed from their respective authentic standards. Since (Z)-4'-OH-TAM, (Z)-4'-END, and (Z)-TAM-N-Oxide did not utilize authentic standards, reported concentrations are relative concentrations; (Z)-4'-OH-TAM and (Z)-4'-END were back-calculated using the (Z)-4-OH-TAM and (Z)-END calibration curves, respectively, and (Z)-TAM-N-Oxide concentrations were back-calculated using the (Z)-4-OH-TAM calibration curve.

Population pharmacokinetic (PK) modeling

A joint parent-metabolite population pharmacokinetic (PK) model was developed in a stepwise manner with sequential addition of metabolites using NONMEM 7.4.1 (ICON Development Solutions, Hanover, MD, USA) interfaced with Pirana 2.9.7 (pirana-software.com). Processing and visualization of NONMEM outputs were performed in R 4.0.3. Individual exposure estimates of area under the concentration-time curve (AUC) and steady-state concentrations (Css) were calculated using simulated profiles in R via the PKNCA package. Between-subject variability (BSV) in the PK parameters was assumed to follow a log-normal distribution. A one-compartment disposition model with first-order absorption and elimination was first developed to describe PK data of the parent drug (TAM). The model was then sequentially expanded by an additional compartment for each metabolite and the PK data were sequentially fitted for each added compartment (Figure S3; Table S6). Since the volumes of distribution of the metabolites were not identifiable and no published data were available at the time of analysis, the volumes of distribution of all the metabolites were considered to be equal to tamoxifen.[22] Proportional random error model was used to quantify the residual unidentified variability (RUV). Potential covariates such as demographics (e.g., body weight, age), smoking, age after menopause, and CYP2D6 metabolizer status were assessed on PK parameters of TAM and its six major metabolites: N-desmethyltamoxifen (NDT), 4-hydroxytamoxifen (4-OHTAM), endoxifen (END), 4'-hydroxytamoxifen (4'-OHTAM), tamoxifen N-oxide (TAM-NOX), and Z'-endoxifen (Z'-END). The final model was selected based upon diagnostic plots, precision of parameter estimates (relative standard error, RSE), and changes in the value of the objective function. Visual predictive checks (VPC) were also used to evaluate the final model by simulation of five hundred replicates of the analysis dataset (see Figure S4). The observed plasma concentration data were overlaid on the 5th, 50th, and 95th percentiles of the simulations to visually assess concordance between the observations and the model-based simulated data. Using the PK parameter estimates from the final model, simulations were conducted to calculate Css of TAM and its metabolites in plasma using exposure estimates AUC after 15 weeks. A total of 301 plasma concentrations (43 time points) from 23 treated subjects were used to simultaneously describe the time course of TAM and its six metabolites using a seven-compartment model with proportional RUV (see Figure S3). Final model parameter estimates and their RSE are provided in Table S6. In the final model, between-subject variability (BSV) could be estimated reliably for the volume of distribution and conversion rate constants of TAM to 4-OHTAM, TAM-NOX, and NDT, as well as elimination rate constants of END and TAM-NOX. Body weight was included as a covariate on the volume of distributions of TAM and metabolites.

Genotyping

Genotyping was performed at the Roswell Park Comprehensive Cancer Center as previously described,[60] using established methods. DNA was extracted from patient blood samples collected at baseline for analysis of single nucleotide polymorphisms (SNPs) in *CYP2D6, CYP3A4 and CYP3A5* genes encoding the respective enzymes that are involved in Tam metabolism. Twenty-one polymorphisms in these three genes were genotyped:18 SNPs from *CYP2D6* including SNPs representing *CYP2D6*2, CYP2D6*3, CYP2D6*4, CYP2D6*6, CYP2D6*9, CYP2D6*10, CYP2D6*41* alleles, and 3 SNPs in *CYP3A4/5* namely *CYP3A4*1B, CYP3A4*18* and *CYP3A5*3*. The SNPs are listed in Table S3. SNP genotyping was performed using the MassARRAY Compact system (Sequenom, San Diego, CA). Briefly, the protocol involved polymerase chain reaction (PCR) amplification of the DNA samples using SNP-specific primers, followed by a base extension reaction using the iPLEX Gold chemistry (Sequenom). All SNP-specific and mass extend oligonucleotides were designed using RealSNP and MassARRAY Assay Designer (Sequenom) and purchased from Integrated DNA Technologies (Coralville, IA). HotStart Taq Polymerase (Qiagen, Santa Clarita, CA) was used for all PCR amplifications. Five nanograms of DNA were added to each 5-μL PCR reaction mixture in 384-well plates. PCR primers were assigned into appropriate multiplex groups by RealSNP and used at a 200 nmol/L final concentration. The PCR condition was set for 94°C for 15 min for hot start, followed by denaturing at 94°C for 20 s, annealing at 56°C for 30 s, extension at 72°C for 1 min for 45 cycles, and final incubation at 72°C for 3 min. The PCR products were treated with 2-μL shrimp alkaline phosphatase (Sequenom) for 20 min at 37°C and then ramped to 85°C for 5 min to remove excess deoxyribonucleotide triphosphates before performing the base extension reaction with Sequenom iplex enzyme and cleaning the products with SpectroCLEAN (Sequenom) resin. All reactions were carried out in a PTC225 thermal cycler (MJ Research, St Bruno, Quebec, Canada). The final PCR products were spotted to the appropriate locations on a 384-pad SpectroCHIP (Sequenom) using a ChipSpotter LT nanodispenser (Samsung, Seoul, South Korea) and analyzed to acquire data by mass spectrometry using the MassARRAY Analyzer Compact MALDI-TOF MS (Sequenom). Genotyping calls were performed in real time by the MassARRAY Typer Analyzer v3.4 (Sequenom).

For quality control purposes, each SNP assay was validated on DNA samples from the Coriell Cell Repository (http://ccr.coriell.org/), SNP 500 DNA set, and three pedigree families to allow identification and removal of poor-quality assays before analyzing experimental samples. Furthermore, DNA samples with known genotypes were included in the sample plates to serve as positive controls during the genotyping assays.

Determination of p53 status in tumor samples

Immunohistochemistry (IHC)

IHC for p53 was performed on the core biopsy specimens after enrollment, but p53 levels were not used as an eligibility criterion. The paraffin block (or 15-5 microns tissue thickness on charged slides) used for ER determination was cut for p53 immunohistochemical staining, using a commercially available antibody detection system (Dako Corporation, Carpinteria, CA), according to the manufacturer's protocol. Targeted DNA sequencing: The p53 status was confirmed in the resected tumor tissue by targeted sequencing of p53. 40–50 mg of each tumor tissue was disrupted using mortar and pestle followed by homogenization with RLT buffer. Homogenized tissue samples processed for DNA extraction using Allprep DNA/RNA/Protein KIT' (QIAGEN-80004) as per manufactures protocol. Quality and Integrity of isolated DNA was analyzed by NanoDrop 8000 (Thermo Scientific) spectrophotometer. DNA sequencing libraries were generated using the TruSeq Custom Amplicon kit (Illumina Inc.), using 250ng of genomic DNA. Amplicons of ~250 bp in length were designed using Illumina Design Studio Software. Custom oligo capture probes flanking the region of interest were hybridized to the genomic DNA. A combined extension/ligation reaction generated the region of interest between the flanking custom oligo probes. PCR was then performed to add indices and sequencing adapters. The amplified final libraries were cleaned up using AmpureXP beads (Beckman Coulter). Purified libraries were quantitated using the KAPA Biosystems qPCR kit and were pooled together in an equimolar fashion, following experimental design criteria. The pooled samples then were then loaded on onto an Illumina MiSeq platform following standard protocols for 2 × 150 cycles.

Immunohistochemical staining and scoring of the human breast cancer tissue micro array (TMA)

TMA construction

Three 1-millimeter tissue cores from each formalin-fixed paraffin-embedded donor blocks were precisely arrayed into a new recipient paraffin block that included tumor specimens and controls. Specimens for controls within the TMA consisted of multiple cores of normal tissue from ten different organs, including the heart, colon, kidney, adrenal gland, ovary, myometrium, brain, thyroid, lung, and prostate, thereby representing more than 20% of all the cores in a TMA. Tumor cores were distributed on to three TMAs, with each tumor core on them represented in triplicate. Appropriate IRB approval consistent with federal, state, and local requirements was obtained for this project, and clinical and outcome data were de-identified.

Immunohistochemistry (IHC)

Formalin-fixed paraffin sections were cut at 4 μm, placed on charged slides, and dried at 60°C for 1 h. Slides were cooled to room temperature and added to the Dako Omnis autostainer, where they were deparaffinized with Clearify (American Mastertech; catalog #CACLEGAL) and rinsed in water. Flex TRS High (Agilent; catalog #GV804) was used for target retrieval for 30 min for the following antibodies; p21, p53, and MDM2. Flex TRS Low (Agilent; catalog #GV805) was used for ESR1. The following list includes primary antibody dilutions and incubation times – p21 (Dako M7202) at 1/25 for 30 min, p53 (Santa Cruz sc-126) at 1/50 for 30 min, MDM2 (Millipore OP46) at 1/50 for 30 min, ESR1 (Santa

Cruz sc-543) at 1/100 for 20 min. HRP (Agilent GV823) was applied to all slides followed by DAB (Agilent; catalog #K3468) for visualization. Slides were counterstained with Hematoxylin, removed from the Omnis, dehydrated, cleared, and coverslipped.

Slide scanning and image analysis

TMA slides were digitally scanned using AperioScanscope (Aperio Technologies, Inc., Vista, CA) with 20× bright-field microscopy. These images are then accessible using Spectrum (Aperio Technologies, Inc., Vista, CA), a web-based digital pathology information management system. Slide images are automatically associated to a digital slide created in the Digital Slide table in Spectrum.

Once slides are scanned, AperioImageScope version 11.2.0.780 (Aperio Technologies, Inc., Vista, CA) was used to view images for image analysis. Slide image data field were populated, images were examined for quality and were amended as necessary. An annotation layer was created for each core of interest in the TMA. Invasive tumor cell-only regions were identified and annotated to appropriately represent the heterogeneity of staining of each TMA core for image analysis. Care was taken to avoid including areas of carcinoma *in situ* and regions with staining artifacts. When possible, representative areas of tumor were selected for analysis with a minimum target of 30 cells per TMA core. Areas of target cells for image analysis were circled using the free form pen tool and areas to be excluded were marked using the negative free form pen to reduce cells irrelevant regions from image analysis calculations. Image analysis data was exported from Spectrum as a tab delimited.csv file and converted to a.xls file and formatted using Microsoft Excel 2010.

Quantitative scoring of immunohistochemistry signals

The nuclear segmentation factor parameter was set to account for brown stain in the nuclear compartment and the nuclear threshold type was set to adaptive, in which allows the algorithm to adjust thresholds based on the strength of the staining. The Nuclear Algorithm detects the positive (DAB) nuclear staining for the individual tumor cells and quantifies their staining intensity. Cell nuclei are individually classified as 0 - none, 1+ - weak, 2+ -moderate, and 3+ -strong. The algorithm uses color de-convolution that separates the hematoxylin and DAB stains, thereby providing stain separation. The analysis results provided the total number of detected cells, the percentage of cells per class (0, 1+, 2+ and 3+) and the percentage of positive stained cells along with the average staining intensity of the positive nuclei as a score of 0, 1+, 2+ and 3+. The H-score score equals = 1*(%1+) + 2*(%2+) + 3*(%3+) with the score is between 0 and 300, where 300 represents 100% of cells being 3+. The counterstain hematoxylin, a blue stain, was applied for morphologic detail of the surrounding tissue to help identify nuclear and cytoplasmic compartments of cells for analysis.

Proximity ligation assay (PLA)

Formalin-Fixed paraffin embedded (FFPE) tissues (arrayed in triplicate in each TMA) on three TMAs (BrCa54, BrCa67 and ATA-54) were deparaffinized in xylene for 3 min and hydrated through an ethanol gradient (3 min in 100%, 3 min in 70%). After hydration, TMAs were washed twice with tris-buffered saline with Tween 20 (TBST) followed by antigen retrieval using antigen retrieval buffer (EnVision FLEX Target Retrieval Solution, High pH (50×) (Dako Omnis) GV804) in steamer at 100°C for 1 h. TMA slides were cooled at room temperature and further quenched by Duolink hydrogen peroxide (Sigma-DUO82054) for 10 min followed by blocking by Duolink blocking solution (Sigma-DUO82007) for 5 min. Primary antibodies of ERα (HC20-1:100) and p53 (DO1-1:100) were diluted appropriately in antibody dilution buffer applied on each TMA (50 µL) and incubated further for 1 h in a humidified chamber. Following the primary antibody incubation, mouse PLUS and rabbit MINUS secondary PLA antibodies were diluted appropriately in antibody dilution buffer and were applied to the TMA (50 µL) and incubated for 1 h in a humidified chamber. The ligation and amplification reactions were carried out on all slides as described by the manufacturer (Sigma-DUO92012A). After amplification, TMAs were incubated with Horseradish peroxidase (HRP)-labeled hybridization probe for 1 h in humidity chamber at 37°C followed by incubation with substates (A, B, C and D) as per the manufacturer protocol (Sigma-DUO92012B). Following two washes of distilled water, TMAs were then counterstained for 1 min in Duolink nuclear stain (Sigma-DUO82059). TMA sections were dehydrated (2 × 3 min in 95% ethanol; 2 × 1 min in 100% ethanol) and transferred to xylene (3 min) and cover slipped using mounting media (Fisher scientific −23425401). After overnight incubation, TMAs were scanned by Leica Aperio ScanScope XT and images were captured using Aperio Spectrum Digital Slide System. ESR1 and p53 interactions signal dots per 300 nuclei in each of the triplicate cores from each patient tumor were counted. Statistical significance of difference in interaction between patients with and without tamoxifen intervention was determined using the Student's t test.

RNA-seq and gene expression analysis

Fifty to eighty mg of each tumor tissue was disrupted using mortar and pestle followed by homogenization with RLT buffer. Homogenized tissue samples processed for RNA extraction using Allprep DNA/RNA/Protein KIT' (QIAGEN-80004) as per manufactures protocol. Extracted total RNA was subjected to DNase digestion using DNase I (Invitrogen- 18068015). RNA Integrity and yield was checked in 1.5% agarose gel and NanoDrop 8000 (Thermo Scientific) spectrophotometer. Sequencing libraries were prepared with the TruSeq Stranded Total RNA kit (Illumina Inc), from 500 ng total RNA. Following the manufacturer's instructions, rRNA was depleted from the total RNA. After ribosomal RNA depletion, the remaining RNA was purified, fragmented, and primed for cDNA synthesis. The fragmented RNA was then reverse transcribed into first-strand cDNA using random primers. Next, the RNA template was removed and a replacement strand was synthesized, incorporating dUTP instead of dTTP to generate double-stranded (ds) cDNA. AMPure XP beads (Beckman Coulter) were used to separate ds cDNA from the second-strand reaction mix, resulting in blunt-ended cDNA. A single 'A' nucleotide was then added to the 3' ends of the blunt fragments.

Multiple indexing adapters, containing a single 'T' nucleotide on the 3' end of the adapter, were ligated to the ends of the ds cDNA, preparing them for hybridization onto a flow cell. Adapter ligated libraries were amplified by PCR, purified using Ampure XP beads, and validated for appropriate size on a 4200 TapeStation D1000 Screentape (Agilent Technologies, Inc.). The DNA libraries were quantitated using the KAPA Biosystems qPCR kit, and were pooled together in an equimolar fashion, following the experimental design criteria. Each pool was denatured and diluted to 16p.m. for On-Board Cluster Generation and 100 paired-end sequencing on a HiSeq2500 sequencer using a paired-end cluster kit and rapid mode SBS reagents following the manufacturer's recommended protocol (Illumina Inc.). Raw feature counts were normalized and differential expression analysis was conducted using 'DESeq2' (Vsn 1.30), and plotted as Volcano Plots using the 'EnrichedVolcano' (Vsn 1.11.3) and as a heatmap using the 'gplots' (Vsn 3.1.3.1) packages in R Statistical Software (Vsn 3.4.1). Differential expression rank order was utilized for subsequent Gene Set Enrichment Analysis (GSEA), performed using the 'clusterProfiler' (Vsn 3.0.4) package in R. Briefly, rank order was established using the 'stat' column from the DESeq2 output of the differential gene expression analysis. Gene sets queried included the Hallmark, Canonical pathways, and GO Biological Processes Ontology collections available through the Molecular Signatures Database (MSigDB). Top pathways from the GSEA output were then visualized as barplots, using the Prism GraphPad (Vsn 7). Furthermore, differentially expressed genes were utilized for master regulator analysis using the 'iRegulon' (Vsn 1.3) application in the Cytoscape Network and Visualization Application (Vsn 2.8.x), which allowed for the generation of networks of the master regulator transcription factors and co-regulators, as well as the transcriptional program these regulators impact.

Reverse phase protein array (RPPA)

RPPA assays with antibodies against proteins or phosphorylated proteins in different functional pathways were carried out as previously described[61,62] at the Antibody-based Proteomics Core Facility at Baylor College of Medicine. Specifically, protein lysates were prepared from 15 to 40 mg of tumor tissue samples using modified Tissue Protein Extraction Reagent (TPER) (Life Technologies Corporation, Carlsbad, CA) and a cocktail of protease and phosphatase inhibitors (Roche, Pleasanton, CA). Lysates were spun at 14,000×g for 15 min at 4°C, and the supernatants were transferred to fresh tubes. The centrifugation was repeated until the supernatants were clear. Protein concentration was determined by BCA assay (PierceTM). Lysates diluted to 0.5 mg/mL were denatured in 2 × SDS sample buffer with 2.5% 2-mer- captoethanol at 100°C for 8 min. The Quanterix 2470 Arrayer (Quanterix, Billerica, MA) with a 40 pin (185 μm) configuration was used to spot samples and control lysates onto nitrocellulose-coated slides (Grace Bio-labs, Bend, OR) using an array format of 960 lysates/slide (2880 spots/slide). The slides were processed and probed with a set of 210 antibodies against total proteins and phosphoproteins using an automated slide stainer Autolink 48 (Dako, Santa Clara, CA, USA). Each slide was incubated with one specific primary antibody, and a negative control slide was incubated with an antibody diluent without any primary antibody. Primary antibody binding was detected using a biotinylated secondary antibody followed by a streptavidin-conjugated IRDye680 fluorophore (LI-COR Biosciences, Lincoln, NE, USA). The total protein content of each spotted lysate was assessed by fluorescent staining with Sypro Ruby Protein Blot Stain, according to the manufacturer's instructions (Molecular Probes, Eugene, OR, USA). Fluorescence-labeled slides were scanned using a GenePix 4400 AL scanner, along with the accompanying negative control slides, at an appropriate PMT to obtain the optimal signal for this specific set of samples. The images were analyzed with GenePix Pro 7.0 (Molecular Devices, Silicon Valley, CA). The total fluorescence signal intensities of each spot were obtained after subtraction of the local background signal for each slide and were then normalized for variation in total protein, background and non-specific labeling using a group-based normalization method as described (Lu et al. 2021). For each spot on the array, the-background-subtracted foreground signal intensity was subtracted from the corresponding signal intensity of the negative control slide (omission of primary antibody) and then normalized to the corresponding signal intensity of the total protein for that spot. Each image, along with its normalized data, was evaluated for quality by manual inspection and control samples. Antibody slides that failed quality inspection were either repeated at the end of the staining runs or removed before data reporting. Triplicate experimental values (normalized signal intensity) (see Table S7) are taken for each sample for subsequent statistical analysis.

Differential protein analysis was performed using the 'limma' (Vsn 3.2.0) linear modeling assessment package in R. Differential proteins ($p < 0.05$) were then correlated with their corresponding transcript levels via the "corrplot" (Vsn 0.92) package, and visualized as a heatmap using the 'gplots' (Vsn 3.1.3.1) package in R Statistical Software (Vsn. 3.4.1). Each protein's association with p53 and ESR1, was then assessed using the STRING-db algorithm, and integrated and mapped with the corresponding transcriptomics data in the Cytoscape Network and Visualization Application (Vsn 2.8.x).

QUANTIFICATION AND STATISTICAL ANALYSIS

Statistical methods

This clinical trial was designed as a randomized window of opportunity pilot trial (NCT01027416) of Tam versus no intervention control (standard of care), employing a blocked randomization scheme and stratified by clinical site. In comparison of the two arms of the clinical trial (Table S3), associations between parameters under each arm were statistically assessed using the Wilcoxon Rank-Sum test (or Kruskal-Wallis test) in the case of ordinal responses and the Pearson Chi-square test for categorical responses.

For Mass spectrometry-based measurement of key metabolites from the Tamoxifen metabolic pathway, mean abundance of metabolites in plasma and tumor samples are reported (Figure 3). p-value was obtained from Student's t test comparing mean plasma and tumor abundance. Data acquisition and quantification was performed using Sciex Analyst software, version 1.6.2. Calibration curves were generated using the analyte/IS area response ratios versus nominal concentration and weighted linear regression with a weighting factor of $1/x2$.

Back-calculated concentrations were generated using the formula $x = (y-b)/m$ where x is the back-calculated concentration, y is the analyte/IS ratio, b is the y-intercept, and m is the slope.

For Covariate analysis in population pharmacokinetic modeling, demographic information (i.e., age, gender, height, and body weight), smoking, age after menopause, and CYP2D6 metabolizer status (e.g., intermediate and normal metabolizers) were considered as potential covariates that might contribute to between-subject variability in PK. Hierarchical models with potential covariates were tested using stepwise forward selection followed by stepwise backward elimination. Changes in objective function value (OFV) were considered significant at $p < 0.01$ (likelihood ratio test, $\chi2$ distribution, 1° of freedom, ΔOFV >6.63) during forward selection and $p < 0.001$ (ΔOFV >10.83) during backward elimination. All potential covariate-PK parameter combinations were tested.

For PLA, ESR1 and p53 interaction signal dots per 300 nuclei in each of the triplicate cores from each patient tumor were counted. Statistical significance of difference in interaction between patients with and without tamoxifen intervention was determined using the Student's t test. Data are represented as mean $\pm$ SEM.

For IHC, an absolute standardized mean difference of 0.792 or larger in percent positive cells is detectable using a two-sample t-test, given $n = 23 + 30$ at alpha = 0.05 (two-sided) and power = 0.80. Missing data due to dropouts were considered missing-at-random. Additional continuous marker data were analyzed using two-sample t-tests and graphically displayed using boxplots. Binary endpoints were compared between treatment arms using Fisher's exact test. Categorical endpoints were compared between treatment arms using Pearson's chi-square test of independence.

For transcriptome analysis, raw feature counts from RNA-seq were normalized and differential expression analysis was conducted using 'DESeq2' (Vsn 1.30), and plotted as Volcano Plots using the 'EnrichedVolcano' (Vsn 1.11.3) and as a heatmap using the 'gplots' (Vsn 3.1.3.1) packages in R Statistical Software (Vsn 3.4.1). Differential expression rank order was utilized for subsequent Gene Set Enrichment Analysis (GSEA), performed using the 'clusterProfiler' (Vsn 3.0.4) package in R. Briefly, rank order was established using the 'stat' column from the DE-Seq2 output of the differential gene expression analysis. Gene sets queried included the Hallmark, Canonical pathways, and GO Biological Processes Ontology collections available through the Molecular Signatures Database (MSigDB). Top pathways from the GSEA output were then visualized as bar plots, using the Prism GraphPad (Vsn 7).

For RPPA, differential protein analysis was performed using the 'limma' (Vsn 3.2.0) linear modeling assessment package in R. Differential proteins ($p < 0.05$) were then correlated with their corresponding transcript levels via the "corrplot" (Vsn 0.92) package, and visualized as a heatmap using the 'gplots' (Vsn 3.1.3.1) package in R Statistical Software (Vsn. 3.4.1). Each protein's association with p53 and ESR1, was then assessed using the STRING-db algorithm, and integrated and mapped with the corresponding transcriptomics data in the Cytoscape Network and Visualization Application (Vsn 2.8.x).